Static and dynamic interactions between Josephson junctions

J. Bindslev Hansen and P. E. Lindelof

Physics Laboratory I, H. C. Ørsted Institute, University of Copenhagen, DK-2100 Copenhagen Ø Denmark

This review covers the experimental and theoretical progress over the last 15 years in the study of systems of interacting Josephson junctions. Such systems are of interest for device applications and for investigations of nonequilibrium phenomena in superconductors. In the description of coupled Josephson elements the emphasis is on the "physics" involved in a number of interaction mechanisms and not so much on the technical problems encountered in the construction of arrays of coupled juntions.

CONTENTS

I. INTRODUCTION

A. The Josephson effects

According to the Ginzburg-Landau theory, the superconducting state of the conduction electron sea can be characterized by a complex order parameter (or wave function) $\psi(\mathbf{r})=\psi_0 e^{i\phi}$ with $\psi_0^2=n_s(\mathbf{r})$, the local density of superconducting electrons.

In a Josephson junction the stationary (dc) Josephson supercurrent I_s is a periodic function of the quantum-mechanical phase difference ϕ between two weakly connected superconductors. In the nonstationary state the voltage V across the junction is proportional to the time derivative of ϕ. The basic Josephson equations are (Josephson, 1962,1964,1965)

$$I_s=I_c\sin\phi \tag{1.1}$$

and

$$V=\frac{\hbar}{2e}\frac{d\phi}{dt}=\frac{\hbar}{2e}\omega_J\ , \tag{1.2}$$

where I_c is the maximum supercurrent the junction can support (typically 1 μA—1 mA). $\nu_J=\omega_J/2\pi$ is the Josephson frequency. The fundamental constant in the voltage-frequency relation (1.2) is

$$\frac{\nu_J}{V}=\frac{2e}{h}=484\ \text{MHz}/\mu\text{V}\ . \tag{1.3}$$

A Josephson junction constitutes a voltage-controlled oscillator capable of generating very high frequencies—up to the energy-gap frequency of the superconductor $\nu_\Delta=2\Delta/h\approx k_B T_c/h$ (typically up to 1000 GHz).

The early work on the Josephson effects was primarily concerned with tunnel junction structures that were, and still are, the best-characterized Josephson junctions. Since then it has become clear that a great variety of superconductor diode structures exhibit the same effects. Figure 1 shows the main types of Josephson junctions.[1] They have all been used in experiments with arrays of coupled junctions—the subject of this review.[2] For recent reviews on the Josephson effects in general, we refer to Waldram (1976) and to Likharev (1979).

---

[1]Throughout this review we shall use the terms *Josephson junction, element,* or *weak link* to mean the same thing.

[2]This review deals only with systems that are of a well-defined *discrete* nature. We do not attempt to cover the literature on collective phenomena in inhomogeneous superconductors. Readers interested in this subject may consult one of the original papers (Parmenter, 1967) or the proceedings of a recent conference on the subject (Gubser *et al.*, 1980).

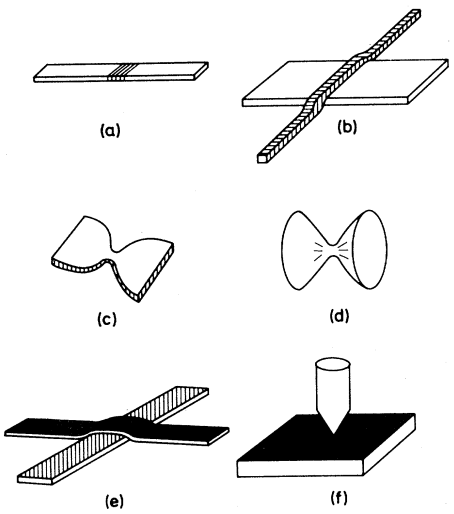

FIG. 1. Different types of Josephson junctions: (a) 1D phase-slip center, (b) proximity effect bridge, (c) 2D microbridge, (d) 3D microbridge, (e) tunnel junction, and (f) point contact.

B. The resistively shunted junction model

Using the two-fluid model of a superconductor there is in a Josephson junction in addition to the supercurrent I_s a contribution I_N from the normal electrons

$$I=I_s+I_N=I_c\sin\phi+\frac{V}{R_N}$$
$$=I_c\sin\phi+\frac{1}{R_N}\frac{\hbar}{2e}\frac{d\phi}{dt}\,. \tag{1.4}$$

Here R_N is the resistance in the junction that the normal electrons see (the quasiparticle resistance). This is the so-called RSJ model (the resistively shunted junction model). This simple model has turned out to be adequate in predicting the principal behavior of Josephson junctions. It is very useful in designing Josephson electronics.

C. Why arrays?

1. General considerations

The study of interacting Josephson junctions has been stimulated by the interest in constructing coherent arrays of junctions for technical applications and by the desire to achieve a better understanding of the fundamental static and dynamic properties of the nonequilibrium state in and around superconducting weak links, noting that these phenomena, which involve rapid temporal and spatial variations of ψ and V, are often most sensitively monitored by using another weak link as detector (Giaever, 1965). Over the last couple of years, large arrays of Josephson junctions have been used to investigate collective behavior of the two-dimensional flux vortex lattice, which is linked to such an array system.

Coherent action of a number of Josephson elements means that the high-frequency Josephson oscillations in all the junctions occur at the same frequency and with the phases locked together. The frequency and phase locking are the hallmarks of a coherent array of Josephson junction oscillators. The apparent similarity to the coherent action of a great number of atomic or molecular oscillators in a laser (or a maser) was noted early on, and the term "superradiance" was used to describe the coherent radiation from a Josephson junction array (Tilley, 1970). However, more recent experimental and theoretical work within this field shows that phase locking between Josepson junction oscillators is well described by the classical theory of phase-locked oscillators and that stimulated emission of photons is apparently not taking place.

2. Applications

From the point of view of applications the Josephson junction constitutes an interesting high-frequency voltage-controlled oscillator with extremely high tuning agility. Furthermore, the nonlinear properties of the junction also make it a sensitive detector and mixer of electromagnetic waves. It is therefore natural that a substantial effort has been spent in applying the Josephson junction in radio frequency (rf) devices like oscillators, detectors, mixers, and parametric amplifiers. The breakthrough for this technology is, however, yet to be seen.

The usefulness of Josephson elements in device applications is limited by a number of factors.

(1) The need to cool the junctions to low temperatures ($T<10$ K).

(2) The inherently low voltage ($V\lesssim 1$ mV) and power level of the junctions.

(3) The high-frequency coupling problem, i.e., the problem of impedance matching low-resistance junctions to the high impedance of conventional microwave transmission lines ($Z_0\approx 10^2\ \Omega$).

(4) The rather fragile nature of many of the existing types of junctions, e.g., their high susceptibility to electrical and/or mechanical shocks or to thermally induced processes.

The first two of these limiting factors are of a fundamental nature. They stem from the small value of the energy gap in superconductors ($2\Delta/e\approx k_BT_c/e\approx 1$ mV) and from the small value of the magnetic-flux quantum $\Phi_0=h/2e=2.07\times 10^{-15}$ V s. The last two factors listed above are more technologically determined. The prospects for overcoming these obstacles to potential applications can be summarized as follows.

(1) Concerning the need for low temperatures, recent developments in small-scale cooling engines seem promising. The construction of systems like the Stirling cryocooler (Zimmerman, 1980; Sullivan *et al.*, 1981) and the miniaturized Linde refrigerator working on the Joule-Thomson cycle (Garvey *et al.*, 1983)—possibly combined with the use of high-T_c superconductors—show the feasibility of the ultimate goal in superconductive electronics: the superconducting device and the refrigerator integrated

into "a single package, the size of a miniature vacuum tube which would be inexpensive, replaceable and disposable" (Little, 1978). The required cooling power is typically 100 mW at 5 K.

(2) As to the second fundamental factor, an array of Josephson elements working coherently in phase could raise the available voltage and power to a useful level, say, 1 V and 1 μW. As we shall see, the state of the art of constructing such arrays has progressed steadily since its start about 15 years ago (Clark, 1968).

(3) The high-frequency impedance-matching problem may be solved using compact, coherent arrays of series-connected junctions combined with microwave coupling structures based on microstrip or on coplanar strip-line configurations made in thin superconducting films (Sørensen *et al.*, 1981).

(4) Arrays of junctions are less vulnerable to electrical burnout than single elements. This is particularly important for microbridges and small-area, high current-density tunnel junctions.

We conclude that the development of miniature refrigeration systems and of coherent arrays of robust Josephson elements would overcome the major limitations to a wider utilization of the Josephson junction.

II. ARRAYS OF JOSEPHSON JUNCTIONS

A. Basic concepts

As stated above, in a coherent array the ac Josephson oscillations in all the junctions are phase locked at the same frequency. The construction of such coherent systems is based on the frequency-pulling and phase-locking effects that arise when the ac Josephson oscillation in a single junction interacts nonlinearly with the high-frequency signal from another source, which can be another Josephson junction or a conventional (room-temperature) rf oscillator. There are thus basically two ways of achieving coherent behavior from an array of elements: either a sufficiently strong high-frequency interaction exists internally between the junctions, pulling them into an *intrinsically* coherent state—provided their voltages (frequencies) are nearly equal—or a sufficiently strong *external* monochromatic rf source can frequency pull and phase lock all the junctions into an externally synchronized coherent state. In this review we shall mainly be interested in the intrinsically coherent Josephson array. In particular, we intend to emphasize the "physics" behind a number of static and dynamic interaction mechanisms that are relevant in systems of coupled Josephson junctions. Such coupling mechanisms naturally fall into two classes: (1) *short-range* interactions, i.e., proximity interactions, within the nonequilibrium region around a junction (Sec. III), and (2) *long-range* coupling, i.e., coupling through external (lumped or distributed) circuit elements (Sec. IV).

B. Array configurations

Irrespective of the synchronizing mechanism involved, Josephson arrays may be characterized by their dc coupling configuration: *series* or *parallel.* Series- and parallel-connected arrays present different technological problems, which, for the sake of clarity, we shall discuss first.

1. Series arrays

For a *series array* to work coherently, the junctions must be almost identical—i.e., the same dc bias current through all the junctions must produce nearly the same dc voltage (frequency) for all the junctions. A high-frequency interaction between the junctions may then pull them all into the desired phase-locked state. Up to now it has not been possible to construct a large number of junctions with identical parameters. The best results so far have been obtained with tunnel junctions. A spread of 10% in I_c for 85% of the junctions is a typical result (Harris *et al.*, 1978; Hebard *et al.*, 1978; Greiner *et al.*, 1980; Davidson, 1981). This fabrication problem arises from the fact that the tunneling probability and hence the junction current depends exponentially on the thickness of the insulating layer.

a. Matched series array

If a *coherent* n-junction series array is impedance matched to the external load, i.e., $R_L = nR_N$, we get the maximum (rms) value of the power available from the array,

$$P_n^{\max,\mathrm{coh}} = n(R_N I_c)^2/8R_N = n^2(R_N I_c)^2/8R_L \quad (\text{for } V > I_c R_N)\,. \tag{2.1}$$

Since $R_N I_c = (\pi/4)(\Delta^2/ek_B T_c)$ is a constant for a given superconductor at a given temperature (Ambegaokar *et al.*, 1963; Aslamazov *et al.*, 1969), we have the important result that for a given load the available power in the coherent, matched case considered here increases proportionally to n^2 (namely, inversely proportional to $R_N = R_L/n$ and proportional to n). Note also that this result favors the use of low-resistance junctions in series arrays (Sandell *et al.*, 1979a). Owing to magnetic self-field effects there exists a lower limit for the resistance of a single junction, $R_N \gtrsim 10$ mΩ (see Sec. II.B.2 below).

If such a coherent impedance-matched series array is made (the reactive components of the impedance should also be matched), the power into a 50-Ω load would be of the order of 5 μW for typical values of the parameters for low-resistance junctions with ideal $R_N I_c$ product ($R_N \approx 0.1\ \Omega$, $R_N I_c \approx 0.1$ mV, $n \approx 500$).

In the case of an *incoherent* series-connected n-junction array, the maximum available power in the impedance-matched case is given by

$$P_n^{\max,\text{incoh}} = n(R_N I_c)^2/8R_L \ , \tag{2.2}$$

i.e., n times smaller than for the corresponding coherent case.

b. Mismatched series array

For an n-junction series array that is *not* matched to the external load—most often because $R_L \gg nR_N$—we have (again for $V > I_c R_N$)

$$P_n^{\text{incoh}} = nP_1 = \tfrac{1}{2}n(I_c R_N)^2/R_L \tag{2.3}$$

for the incoherent case, and

$$P_n^{\text{coh}} = n^2 P_1 = \tfrac{1}{2}n^2(I_c R_N)^2/R_L \tag{2.4}$$

for the in-phase coherent case.

2. Parallel arrays

In a *parallel-connected* array with superconducting connections between the elements, the junctions need not be identical. Since the dc voltage is the same across all the junctions, they will all have the same period of oscillation. In such a parallel array, however, the junctions will in general shunt each other out unless reactive decoupling circuit elements are used. Generally, the impedance will therefore be just R_N/n—i.e., the impedance mismatch to the surroundings will increase. Also, the self-induced magnetic field of the bias current of the array will set an upper limit to the critical current of the system. This will be of the order of 50 mA—i.e., there will never be any desire to match impendances smaller than about 10 mΩ (assuming an ideal $R_N I_c$ product of about 0.5 mV for the junctions).

Even if the self-field can be neglected, another phenomenon is encountered in arrays of parallel-connected junctions. This is the fundamental quantization of the magnetic flux (the fluxoid) threading the large number of superconducting loops inherent in such a system. An array of n junctions in parallel can be thought of as $n-1$ coupled two-junction SQUID's.[3] In such a system, the phase difference between the oscillations in the junctions will be modulated by an externally applied magnetic flux through the loops. In general, with n *nonidentical* junctions, this phase modulation produces randomly distributed phase differences between the junctions that will counteract attempts to establish a state of in-phase coherence between the Josephson oscillators by means of some *other* high-frequency phase-locking currents. The existence of screening currents and flux quantization has therefore been considered an obstacle. These effects have been diminished by increasing the loop inductance and thereby decreasing the magnitude of the fluxoid currents to a level well below that of the phase-locking currents.

In the ideal, somewhat hypothetical, case of n *identical* parallel-connected Josephson junctions constituting $n-1$ coupled symmetrical two-junction SQUID's the junctions will oscillate coherently in phase if the magnetic flux through each of the loops is equal to a multiple of the flux quantum $\Phi = n\Phi_0 = nh/2e$. On the other hand, if the flux through each loop is equal to $\Phi_0/2$ (modulo Φ_0), the phase difference between adjacent junctions will be π—i.e., each pair of junctions will oscillate coherently in antiphase.

It is worth noting that if such an ideal system with n identical parallel-connected junctions could be made and if all the loop areas were the same and the junctions were equally spaced, the resulting array device would constitute an interesting flux-tuned directional microwave source. Such a highly symmetrical array interferometer would be closely analogous to an optical-diffraction grating with continuously variable spacing of the scattering centers (e.g., the grooves). The sharply peaked spatial interference pattern could be controlled by applying a uniform magnetic field to the array, thereby introducing small constant phase shifts between adjacent Josephson oscillators in the array.

Such an array would, of course, also constitute a sensitive magnetometer. As noted by Feynman (1965, p. 21-18), its flux sensitivity could be greatly enhanced over that of a single symmetrical two-junction SQUID (cf. de Waele *et al.*, 1968, and Silver *et al.*, 1979,1981). Since the energy sensitivity of two-junction SQUID's has now reached the quantum level $\sim h$ (Planck's constant), there seems at present to be no reason to use multiple-junction SQUID's in order to enhance the sensitivity.

III. SHORT-RANGE INTERACTIONS

A. Nonequilibrium superconductivity

In a superconductor a nonequilibrium state may be generated by injection of normal electrons (quasiparticles), by changing the energy of the quasiparticles or by breaking pairs. This disequilibrium state will relax through elastic scattering processes, inelastic (mostly electron-phonon) interactions, and diffusion (if possible). A Josephson junction in the voltage-sustaining state carries a quasiparticle current that generates such a nonequilibrium state. This is particularly the case of high current-density junctions like microbridges. In contradistinction to large Josephson tunnel junctions, with low current-density, whose properties are described well by tunneling theory, the voltage-sustaining state of microbridges and of other high current-density weak links has not yet been covered by any complete, generally accepted theory. The reason for this lies precisely in the nonequilibrium state generated in and around Josephson junctions with high current density. The nonequilibrium situation is complex. It consists of coupled nonequilibria in three systems: the pair con-

[3]SQUID is an acronym for superconducting quantum interference device; see Sec. IV.C.

densate, the quasiparticle system, and the phonons, all of which are undergoing rapid temporal and spatial variations in the weak link. Owing to the different relaxation mechanims involved, these variations take place on different time and length scales in the three systems. Hence elements of the theory for superconductors out of equilibrium must be added to the Ginzburg-Landau theory to form the basis for a detailed description of the properties of high current-density weak links. The same theoretical framework is also, of course, needed to describe short-range interactions between two or more of these weak links that are located so close together that their nonequilibrium regions partly overlap. We shall therefore now, before proceeding with a review of short-range interactions between weak links, give a short survey of the characteristic times and lengths associated with the nonequilibrium around a weak link. We shall look at an idealized junction, the one-dimensional phase-slip center [see Fig. 1(a)]. Such "quantized" resistive structures develop in a one-dimensional superconducting strip or filament when the current exceeds the critical value at a particular point along the strip (Notarys *et al.*, 1971, Meyer *et al.*, 1972, and Skocpol *et al.*, 1974). For recent reviews on nonequilibrium superconductivity see Tinkham (1979), and Gray (1981).

B. Characteristic length and time scales in equilibrium and nonequilibrium superconductivity

1. Order parameter

A supercurrent through a superconducting filament will depress the order parameter ψ. For currents above the critical value for the strip, a deep suppression will occur spontaneously at one (or more) points along the filament (this occurs even in a perfectly homogeneous filament). The order parameter will be suppressed over a length determined by the temperature-dependent coherence length $\xi(T)$, of the superconductor [example, in "dirty" tin at $T=0.99T_c$, $\xi(T)\approx 3\ \mu$m].

2. Supercurrent

The supercurrent I_s runs only in a surface layer of the filament given by the London penetration depth, $\lambda(T)$. This is the so-called Meissner effect in superconductors, i.e., the perfect diamagnetism of a bulk superconductor [example, in "dirty" tin at $T=0.99T_c$, $\lambda(T)\approx 2\ \mu$m]. The supercurrent response time τ_J is given by $\tau_J=\tau n/n_s$ ($=2k_BT_c\hbar/\pi\Delta^2$ in the dirty case). Here τ is the elastic relaxation time and n_s/n is the fraction of the conduction electrons that belong to the superfluid.

3. Quasiparticle charge imbalance

If the current through the strip or filament exceeds the critical value, a voltage appears across the phase-slip center and the amplitude of the order parameter oscillates with the Josephson frequency ν_J [Eq. (1.3)]. The oscillation of the order parameter will create a nonequilibrium distribution of the excitations (the quasiparticles) out of the superconducting ground state. Since a redistribution of excitations in energy takes place over a characteristic time of the order of the inelastic (energy) relaxation time, τ_E ($\approx 10^{-10}$ s for tin at $T\approx T_c$), the length scale for variation of properties pertinent to the nonequilibrium excitations will normally be much longer than the coherence length (Pippard *et al.*, 1970). The changing voltage across a phase-slip center implies that the excitations must change their electrochemical potential μ_{qp} relative to the pair condensate. This again implies a quasiparticle charge imbalance Q^* (as will be discussed in the next subsection). Such a quasiparticle charge imbalance decays over a characteristic time

$$\tau_{Q^*}=\frac{4k_BT}{\pi\Delta(T)}\tau_E\approx\frac{\Delta(0)}{\Delta(T)}\tau_E\propto\left[\frac{1}{T_c-T}\right]^{1/2}. \tag{3.1}$$

The corresponding quasiparticle charge imbalance diffusion length is (Tinkham *et al.*, 1972; Waldram, 1975)

$$\Lambda_{Q^*}=(D\tau_{Q^*})^{1/2}\approx[\tfrac{1}{3}v_F^2\tau\tau_E\Delta(0)/\Delta(T)]^{1/2}$$
$$\approx 10\ \mu\text{m}\ \ \text{(in tin)}, \tag{3.2}$$

where v_F is the Fermi velocity of the metal, τ is the usual momentum-transport relaxation time in the metal (the elastic relaxation time), and $D=\frac{1}{3}v_F^2\tau$ is the diffusion constant. The quasiparticle resistance of a one-dimensional (1D) phase-slip center is determined by Λ_{Q^*}. The length of the center can be taken to be $2\Lambda_{Q^*}$. The spatial variation of μ_{qp} over Λ_{Q^*} has been observed directly by Dolan *et al.* (1977), Skocpol *et al.* (1981), and Aponte *et al.* (1983) in tin strips and by Stuivinga *et al.* (1981) in aluminum strips. They also verified the temperature dependence of Λ_{Q^*} inherent in Eq. (3.2)

$$\Lambda_{Q^*}\propto\left[\frac{1}{T_c-T}\right]^{1/4}. \tag{3.2'}$$

4. Neutral quasiparticle energy imbalance

The excitations may, however, also just be redistributed from their thermal energy distribution. Such a neutral energy imbalance decays with the inelastic relaxation time, τ_E. Hence the corresponding diffusion length is

$$\Lambda_E=(D\tau_E)^{1/2}=(\tfrac{1}{3}v_F^2\tau\tau_E)^{1/2}. \tag{3.3}$$

For dirty tin, as above, we have $\Lambda_E\approx 5\ \mu$m (note that Λ_E is only slowly varying with the temperature). The nonthermal energy distribution of the excitations may lead to a suppressed as well as an enhanced energy gap. The effect on the energy gap is sometimes characterized by an effective temperature T^* which corresponds to that equilibrium temperature where the energy gap would have the same value.

5. Phonons

In a superconducting filament suspended in a vacuum, the Joule heat generated at the phase-slip center can escape only through the ends. The temperature will therefore vary linearly from the phase-slip center towards the two ends. In the case when there is a good thermal contact with the substrate (or the helium bath), the temperature will naturally decrease much faster from the value at the phase-slip center towards the substrate (or bath) temperature. Usually, however, the acoustic matching between the thin metal film and the substrate/helium is poor. The phonons are therefore trapped in the film. For such a one-dimensional system a simple heating model was developed by Skocpol *et al.* (1974) and Skocpol (1981). In this model the electrons and the phonons are characterized by the *same* elevated equilibrium temperature. If K is the thermal conductivity of the strip and if α is the heat transfer coefficient across the interface (the Kapitza conductance), then the temperature will decay towards the bath temperature over a characteristic length $\eta=\sqrt{Kt/\alpha}$, where t is the thickness of the metal film. For an indium or tin film with a thickness of 100 nm on a glass substrate one finds roughly $\eta\approx 5\ \mu$m. If the dissipation in the phase-slip center raises the temperature above the transition temperature, a normal "hot spot" is created. A superconductor-normal-superconductor (SNS) junction is formed. The Josephson effects are eventually quenched when the normal region grows to break the coherence between the two superconductors.

The relaxation around a two-dimensional bridge with dimension L will be somewhat faster, since a logarithmic factor $\ln(L/r+1)$ will be multiplied on all the exponential functions of the distance r from the bridge middle. A three-dimensional bridge will have the spatial variation "speeded up" by a factor L/r. This means that the quasiparticle charge imbalance length Λ_{Q^*} will not be determining the electrical resistance of the 3D microbridge (Tinkham *et al.*, 1977; Bindslev Hansen *et al.*, 1980). To give a qualitative idea of the five characteristic lengths, λ, ξ, Λ_{Q^*}, Λ_E, and η, we have made an instantaneous picture of the situation around a 1D phase-slip center, Fig. 2.

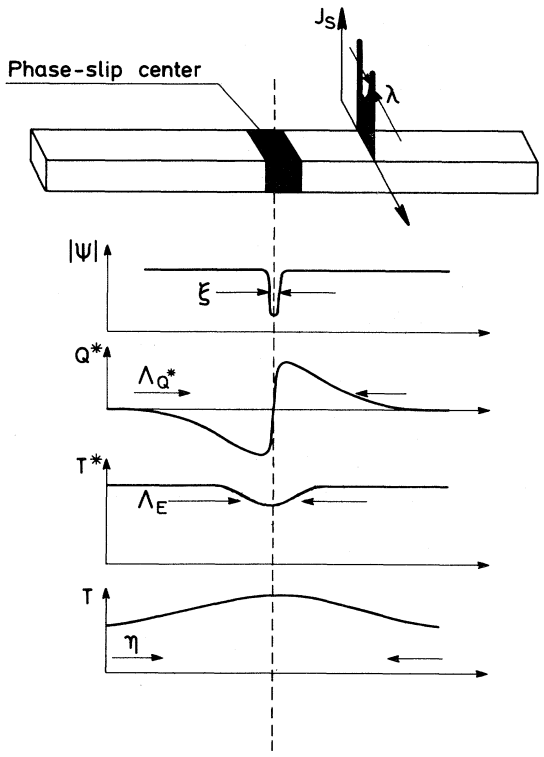

FIG. 2. Spatial variation of the relevant parameters around a one-dimensional phase-slip center (PSC) illustrating the important characteristic lengths in nonequilibrium superconductivity. From the top: the supercurrent density J_s across the strip (λ); order parameter $|\psi|$ variation (ξ); quasiparticle charge imbalance Q^* (Λ_{Q^*}); effective temperature, T^* of the quasiparticle distribution (Λ_E); and the equilibrium temperature T of the lattice (η).

C. Short-range interactions between two weak links

We shall now deal with two closely spaced weak links or phase-slip centers located in the same superconducting medium and interacting through (i) *order parameter variations,* and (ii) *quasiparticle diffusion currents.* The simple RSJ model is not in general capable of giving an adequate description of such proximity coupled weak links. The RSJ model is derived on the basis of the time-independent Ginzburg-Landau (GL) equations in combination with the (time-dependent) Schrödinger equation (Aslamazov *et al.*, 1969). It is used to describe the time variation of the voltage across the weak link. This model, in fact, describes a nonequilibrium situation in the weak link where a quasiparticle charge imbalance is created and released only by currents in the superfluid and in the normal fluid *separately* (by diffusion) and not by relaxation (i.e., $\tau_Q\rightarrow\infty$). To give a better description, the nonequilibrium situation in the immediate vicinity of the weak link, as described in Sec. III.B above, must be taken into consideration.

1. dc order-parameter interaction

When the distance d between two weak links is of the order of the coherence length $d\approx\xi$ each of the links can feel the order parameter variations taking place in the center of the adjacent junction. In the stationary (zero voltage) state, where the order parameter ψ depends only on position and not on time, this interaction is caused by the supercurrent-induced depression of the order parameter which reduces the critical current in the vicinity. Close to T_c, this dc interaction can be fully described by the Ginzburg-Landau (GL) equations with appropriate boundary conditions. For single weak links smaller than ξ these equations give the well-known sinusoidal current-phase relation [Eq. (1.1)] with a predictable critical

current.[4] According to such calculations, the supercurrent suppresses the pair density (the order parameter) in a region extending over a coherence length around the middle of the weak link. For two (or more) closely spaced weak links ($d \approx \xi$) connected in series, the GL equations were solved numerically by Blackburn *et al.* (1972,1975) and Howard *et al.* (1975), and by a perturbation method by Demoniva *et al.* (1979). Figure 3 is a simple one-dimensional picture of the geometry and the spatial variation of ψ [after Jillie (1976)].

The supercurrent-induced depression of the order parameter will depend on the current distribution in the region between the weak links. For the opposed-biased case (with supercurrents flowing in opposite directions through the weak links) the supercurrents will tend to cancel each other in the interlink region. Way *et al.* (1977) solved the equations for both supercurrent configurations [series-biased ($\rightarrow\rightarrow$) and opposed-biased ($\rightarrow\leftarrow$)]. They found that the depression of the critical currents ΔI_c was typically 10% smaller with the currents in opposite directions (opposed-biased) than with the currents in the same direction (series-biased). The observed ΔI_c reported by Jillie (1976) showed only qualitative agreement with the theory (the observed asymmetry in ΔI_c was 30—50 %). Figures 4 and 5 show the sample geometry used by Jillie and the results of the ΔI_c measurements (here both for $V=0$ and $V\neq 0$; we shall return to the latter case in Sec. III.C.3). The measured temperature dependence of the dc order-parameter interaction is plotted in Fig. 6. The interaction is strongest close to T_c where ξ is long. A related phenomenon is the "locking" of the critical currents of two bridges reported by Jillie *et al.* (1976) [and by Octavio *et al.* (1979)]. This phenomenon may intuitively be viewed as a mutually reinforced depression of the order parameter in the two bridges. Figure 7 gives an example of such an observation. Similar results were obtained by Neumann *et al.* (1982), who interpreted their observation of critical current locking in terms of the modulation of I_c of the stronger of the two junctions by the high-frequency radiation from the junction with the lower I_c.

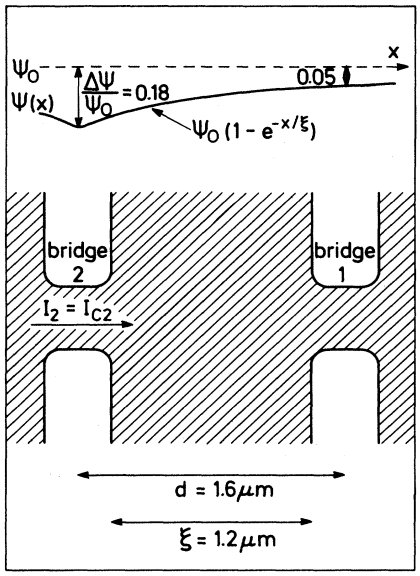

FIG. 3. dc order-parameter interaction. Both weak links are in the stationary state. The figure shows a simple 1D case with $I_2=I_{c2}$ and $I_1=0$. According to the GL theory the maximum supercurrent through bridge 2 causes a depression of the order parameter to 82% of its unperturbed value ($\psi^2=\frac{2}{3}\psi_0^2$). ψ recovers exponentially as shown in the upper part of the figure. In the example shown, with $d=1.6$ μm and $\xi=1.2$ μm, ψ is suppressed by 5% in the unbiased weak link 1 (after Jillie, 1976).

2. ac order-parameter interaction

In the nonstationary state, when finite voltages develop across the two weak links, the order parameter interaction becomes much more complex and, in addition, other interaction mechanisms come into play (charge imbalance currents, lattice heating, and/or an excess of "hot" quasiparticles). The order parameter in the middle of the weak links goes to zero periodically with the Josephson frequency. Its time average $\langle\psi\rangle$ in the center of a weak link will be lower than in the stationary state, and the corresponding depression of $\langle\psi\rangle$ in the other weak link will also be deeper than in the stationary state. The depression in the critical current ΔI_c of one weak link will consequently increase rapidly as the other weak link passes from the stationary zero-voltage state into the nonstation-

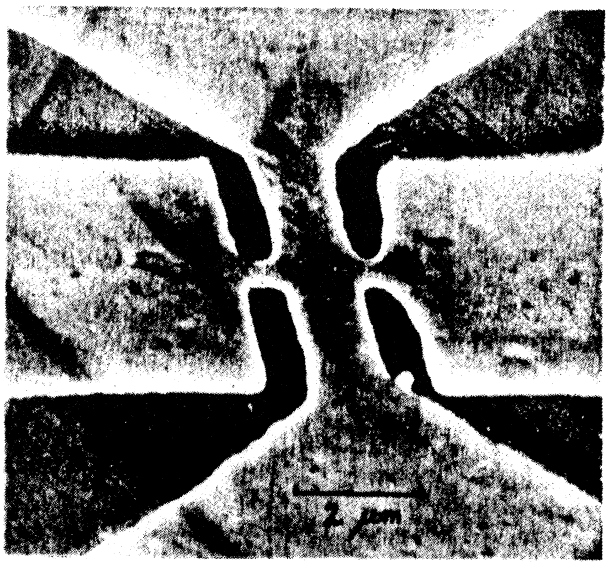

FIG. 4. Scanning electron microscope picture of two indium thin-film microbridges made with electron beam lithography technique (Jillie *et al.*, 1975). The light areas are 100 nm indium film. The bridge separation d is here 1.2 μm.

[4]Effects of the magnetic self-field of the current are neglected. This is justified for weak links smaller than the Josephson penetration depth, λ_J. For thin-film microbridges this condition is normally fulfilled, since $\lambda_J \approx \lambda > \xi$ for thin films (type-II superconductors).

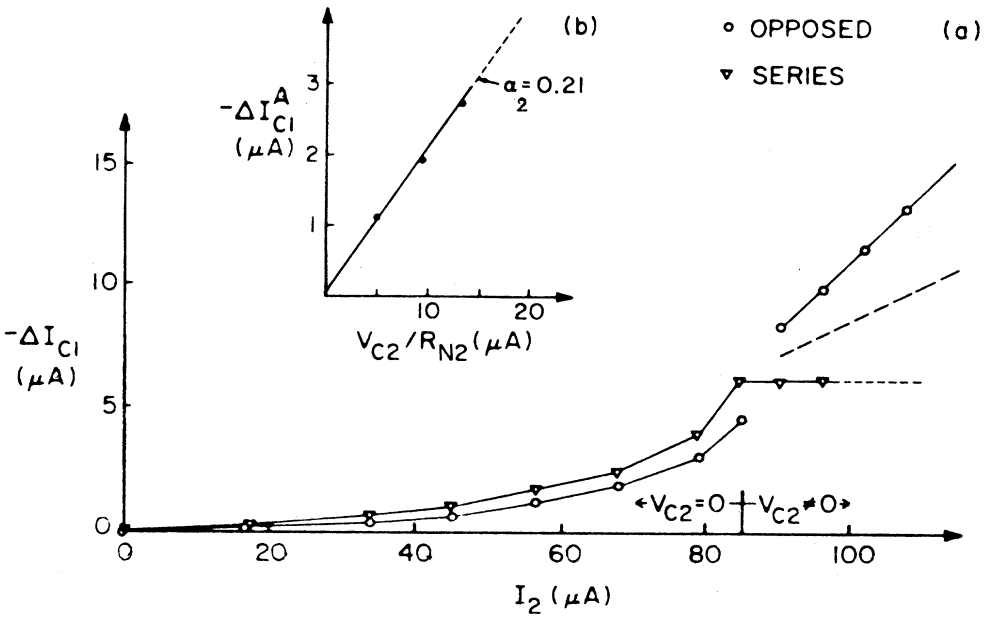

FIG. 5. Experimental results for two proximity-coupled indium microbridges ($d \approx 2$ μm), showing the dc interactions explained in Figs. 3 and 8. (a) the measured change ΔI_{c1} in the apparent critical current of bridge 1 as a function of the current through bridge 2. The data include both current configurations (series biased and opposed biased). The voltage across bridge 2 for $I_1 = I_{c1}$ is denoted V_{c2}. For $I_2 < 85$ μA both bridges are in the stationary state ($V_{c2}=0$), and the dc order-parameter interaction (Fig. 3) is observed. For $I_2 > 85$ μA the dc quasiparticle interaction (Fig. 8) is seen (see Sec. III.C.3). The dashed line (long-dash marks) is the symmetric or average component of ΔI_{c1} for the two directions of I_2. (b) Inset: the *anti*symmetric component ΔI_{c1}^{A} of ΔI_{c1} as a function of $I_{qp2} = V_{c2}/R_{N2}$ ($R_{N2}=0.32$ Ω), the quasiparticle part of I_2. The slope of this plot yields the coupling parameter α_2 (Jillie *et al.*, 1977b).

ary voltage-sustaining state.

Naturally there also exists a high-frequency interaction between two weak links less than ξ apart and both biased at finite voltages. The order-parameter oscillation in one weak link modulates ψ in the other weak link directly. If the two dc voltages are nearly equal (or one is close to a simple fraction of the other), the ac Josephson oscillations in the two weak links will tend to phase lock. This dynamic interaction was treated in detail by Deminova *et al.* (1979), who extended their perturbation calculation to the nonstationary state with current control. In their solution to the GL equation the interaction took the form of a first-order correction to the zero-order approximation which was the well-known solution to the Laplace equation $\nabla^2\psi = 0$ with the usual boundary condition $\nabla_\perp \psi = 0$. They sought solutions describing the phase-locked system with the two weak links running at a single frequency and obtained curves representing the boundaries of the phase-locked regions in currents and voltages for both current configurations and for various values of the coupling

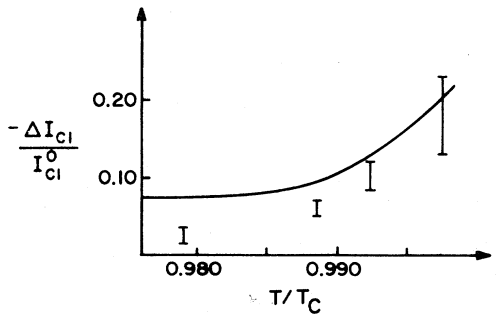

FIG. 6. Measured temperature dependence of the dc order-parameter interaction (Jillie, 1976). The change in critical current ΔI_{c1} is plotted as a function of reduced temperature T/T_c. ΔI_{c1} is taken at $I_2 = I_{c2}$. The spread in ΔI_{c1} is due to the difference in ΔI_{c1} for the two current configurations. The solid line is the theoretical estimate based on the simple picture given in Fig. 3 (1D GL theory).

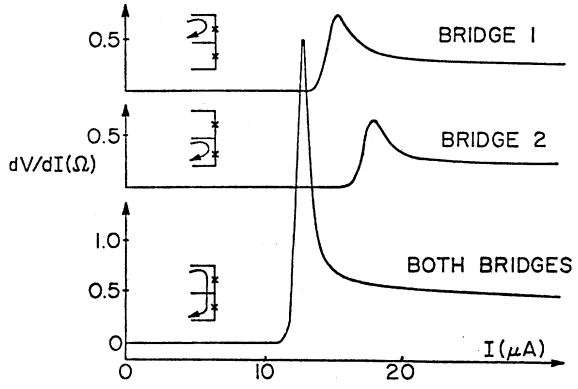

FIG. 7. Measured critical current locking between two indium microbridges 2 μm apart (Jillie, 1976). Note the reduction in the critical currents and the sharpening of the resistive transition when both bridges are biased in series as compared to being biased alone.

strength and of the ratio between the two critical currents. They predicted that for strongly coupled planar thin-film microbridges the widest locking range $\Delta I_{\rm lock}$ should be observed for the opposed-biased current configuration. For pairs of point contacts or variable-thickness bridges (VTB) (in which the coupling would be weaker), the opposite should be the case—i.e., the coupling should be stronger for the series configuration. So far, there are no reports on measurements that could test these predictions for the asymmetrical ac order-parameter interaction.

The upper cutoff frequency for this dynamic interaction will be of the order of the gap frequency $\nu_{2\Delta}=2\Delta/h$. Even close to T_c this limit is so high (e.g., $\nu_{2\Delta}\approx 90$ GHz in indium at $0.99T_c$) that very well-cooled weak links (VTB's or point contacts) would have to be used in order to reach it. In the samples of closely spaced planar microbridges studied so far, heating effects would interfere with the dynamic direct order-parameter interaction already at low voltages (frequencies). In order to distinguish between such an interaction and the ac quasiparticle charge imbalance interaction—which we shall deal with a little later—a very careful study of the frequency and spatial dependence of the coupling would be needed for a pair of well-cooled weak links. In this connection we note that any type of short-range interaction is strongest precisely between planar weak links that do not fulfill the rigid boundary conditions well, i.e., between structures without current concentration, and that these types of junctions are also the ones in which the heating effects are most severe (Likharev, 1979; Tinkham *et al.*, 1977). The voltage-locking interaction observed by Jillie *et al.* (1977b) in their pairs of planar microbridges did exhibit the same form of symmetry as predicted by Deminova *et al.* (1979) (opposed-biased stronger). The much stronger interaction via the ac quasiparticle currents that we shall now turn to is, however, a more likely cause of the observed phenomena.

3. Quasiparticle interaction

In this section we will consider the case of two weak links with one or both of them in the voltage-sustaining state and placed so close together in the same superconducting medium that their nonequilibrium regions overlap—i.e., the oscillating quasiparticle potential and charge imbalance current around one weak link can be felt by the adjacent junction. This requires that $d \lesssim \Lambda_{Q^*}$. A very simple description of this interaction is obtained by including in the RSJ model the quasiparticle currents injected from one bridge into the other (Jillie *et al.*, 1980). The equations are (for the opposed-biased case)

$$I_1+i_{q2}=I_{c1}\sin\phi_1+\frac{V_1}{R_{N1}} \tag{3.4}$$

and

$$I_2+i_{q1}=I_{c2}\sin\phi_2+\frac{V_2}{R_{N2}}\ , \tag{3.5}$$

where i_{q2} is the part of the quasiparticle current generated in bridge 2 that flows through bridge 1—and similarly for i_{q1}. R_{N1} and R_{N2} are the normal-state resistances of the two junctions. The total quasiparticle current through junction 2 is

$$I_{q2}=I_2-I_{c2}\sin\phi_2+i_{q1}\ , \tag{3.6}$$

of which a fraction α_2 flows through junction 1

$$i_{q2}=\alpha_2 I_{q2}=\alpha_2(I_2-I_{c2}\sin\phi_2+i_{q1})\ , \tag{3.7}$$

and similarly for i_{q1}

$$i_{q1}=\alpha_1 I_{q1}=\alpha_1(I_1-I_{c1}\sin\phi_1+i_{q2})\ . \tag{3.8}$$

Combining these equations and assuming that the coupling parameters α_1 and α_2 are small, so that all terms in $\alpha_1\alpha_2$ may be neglected, we have

$$I_1=I_{c1}\sin\phi_1+\frac{V_1}{R_{N1}}-\alpha_2(I_2-I_{c2}\sin\phi_2)\ , \tag{3.9}$$

$$I_2=I_{c2}\sin\phi_2+\frac{V_2}{R_{N2}}-\alpha_1(I_1-I_{c1}\sin\phi_1)\ . \tag{3.10}$$

Using simple substitutions, Jillie *et al.* (1980) showed that these equations are the same as the ones describing a system of two weak links shunted by a common external resistor (see Sec. IV.B).

For large values of α_1 and α_2, we should expect this analogy to break down, since in that case there will be non-negligible feedback currents, meaning that each of the weak links will be affected by the quasiparticle current it injects into the other one. In the nonstationary situation these feedback currents, which also contain information of the phases, become important for the locking mechanism for even small α's.

From a more general point of view, the use of the RSJ model in this simple picture of the quasiparticle interaction implies that the spatial and dynamic characteristics of the nonequilibrium situation around the weak links will not be correctly described (conversion from quasiparticle current to pair current *does* take place in the interlink region). Already for that reason we expect only rough agreement between the experimental results and the predictions of this model. However, the very complex character of the nonequilibrium situation around the weak links requires such a simple picture to get anywhere at all.

A consequence of this model is that a finite voltage across weak link no. 2 will influence the critical current of weak link no. 1, and vice versa. Although this is a simple consequence of Eqs. (3.9) and (3.10), we shall present a qualitative argument, as illustrated in Fig. 8. As shown, weak link no. 2 is biased at a voltage which drives a proportional quasiparticle current $I_{\rm qp2}=V_2/R_{N2}$. A small fraction $\alpha_2 I_{\rm qp2}$ of this current is injected through weak link no. 1. Link no. 2 is shown biased in the same direction as weak link no. 1 (series) or in the opposite direction (opposed-biased). If weak link no. 1 carries only a supercurrent ($I_{\rm qp1}=0$), the maximum zero-voltage current will

be the sum of the intrinsic critical current of weak link no. 1 and $\alpha_2 I_{qp2}$. Therefore, in the series case the (apparent) critical current I_{c1} will be larger (by $\alpha_2 I_{qp2}$) than the intrinsic value—and in the opposed-biased case it will be smaller by the same amount. This is the antisymmetrical dc quasiparticle interaction reported by Jillie *et al.* (1977a); see Fig. 8. They found a coupling constant $\alpha_2 \approx 0.2$ for a pair of planar indium microbridges placed $d = 2$ μm apart. With $d = 4$ μm between two indium bridges they observed $\alpha_2 \approx 0$ (i.e., no coupling). More recently, Dai *et al.* (1982) found $\alpha_2 \approx 0.8$ for $d = 0.5$ μm and a very restricted geometry between their pair of indium bridges.

A similar, although less transparent, stationary interaction is expected in the case when both weak links are biased at a finite voltage ($I_{qp1} \neq 0$ and $I_{qp2} \neq 0$ in Fig. 8). Again an antisymmetrical interaction based on the injected diffusive quasiparticles will help the total currents I_1 and I_2 in the series configuration and hamper them in the opposed-biased case. The two bias current configurations will also give a different quasiparticle potential μ_{qp} in the region between the weak links, as illustrated in Fig. 9. The pair potential μ_p has no anomalies in the interlink region as long as the weak link separation d is much greater than the coherence length ξ (note that $\xi < \Lambda_{Q^*}$).

The effect of the second-order terms proportional to $\alpha_1 \alpha_2$ was considered by Neumann *et al.* (1981), who found a suppression of the critical current of one junction caused by the ac quasiparticle current flowing through the other junction. The effect was independent of the relative current directions.

At this point it seems appropriate to discuss the effect that the dimensionality of the system may have on the interaction strength. For short-range interaction experiments planar (2D) microbridges may be superior to the more well-cooled quasi-three-dimensional microbridges (VTB). The fact that the two-dimensional geometry lets the temperature drop only slowly from the weak link out into the background film (Tinkham *et al.*, 1977) means

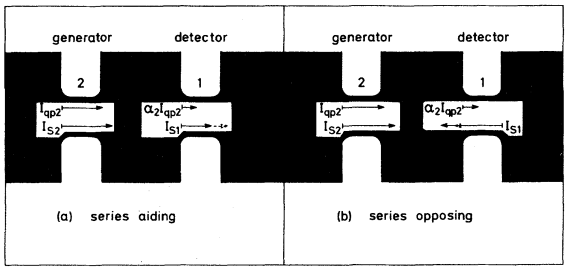

FIG. 8. Asymmetrical dc quasiparticle interaction between two closely spaced microbridges. Both current configurations, series biased and opposed biased, are shown for the case where $I_2 > I_{c2}$ and $I_1 < I_{c1}$. A fraction α_2 of the quasiparticle current through bridge 2 is injected through bridge 1. In the series configuration this injected current $\alpha_2 I_{qp2}$ adds to the intrinsic critical current of bridge 1 and therefore enhances the measured (apparent) critical current. In the opposed-biased case the injected current subtracts from the intrinsic critical current.

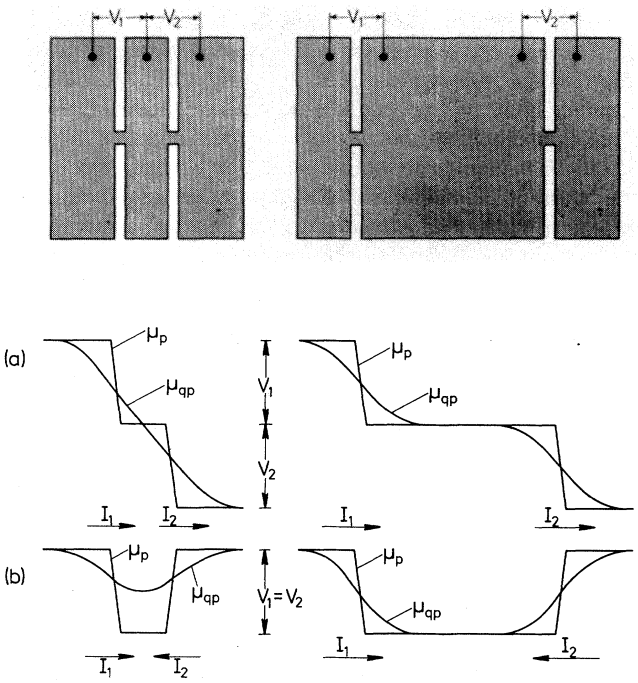

FIG. 9. Qualitative picture of the instantaneous variation of the pair potential μ_p and the quasiparticle potential μ_{qp} in the region around two closely spaced microbridges (shown in the upper part of the figure). The variations are shown for two different interbridge spacings and for both current configurations, (a) series biased, and (b) opposed biased (Lindelof *et al.*, 1981).

that the quasiparticle potential also drops slowly. The implication is that a pair of two-dimensional microbridges will interact over a somewhat longer distance than three-dimensional (or quasi-3D) microbridges. In particular, if the heat flow across the interface between the film and the substrate is appreciable, two-dimensional weak links should interact more strongly via the oscillating quasiparticle potential than weak links in variable-thickness geometries that allow for a rapid diffusion of quasiparticles, thus "diluting" the nonequilibrium quasiparticles around the bridges. One-dimensional systems should exhibit even stronger coupling phenomena. The measurements reported by Meyer *et al.* (1977) of coupled phase-slip centers in tin whisker crystals seemed to confirm this, and the recent, extensive study of interacting phase-slip centers in a one-dimensional tin strip by Aponte *et al.* (1983) clearly showed the longer range of the dc quasiparticle interaction. For $d = 2$ μm the measured value of the coupling strength in this one-dimensional system was $\alpha \approx 0.7$. In their two-dimensional indium system Jillie *et al.* (1977) found $\alpha \approx 0.2$ for $d = 2$ μm.

The nonequilibrium quasiparticle distribution created in the common electrode between two tunnel junctions may be used to obtain a device with current gain. The gain stems from an enhancement of the tunneling current in the detector junction caused by the quasiparticles injected into the common electrode by the generator junc-

tion (cf. Fig. 16). For moderate injection currents, Gray (1970) achieved a current gain of about 4. Using very strong injection currents that suppress the energy gap significantly, Faris *et al.* (1983) have obtained higher gain (≈ 8) in their so-called "Quiteron." Work along the same lines has recently been reported by Hunt *et al.* (1983), who have made a faster device (but with correspondingly smaller gain) using two small Nb junctions less than 0.1 μm apart in a geometry that allows rapid diffusion of the quasiparticles out of the common electrode.

4. Voltage-locking quasiparticle interaction

When the voltages across two closely spaced weak links have the same absolute value (or one is a simple multiple of the other), their ac Josephson oscillations can become synchronized and their voltages can lock together over some finite current range ΔI_{lock}—see Figs. 10 and 11, where results taken from Jillie *et al.* (1980) and Lindelof and Bindslev Hansen (1977b) are reproduced. Such voltage-pulling and -locking phenomena are also predicted by the simple model discussed above. This is illustrated in Fig. 12, which shows some of the results of computer simulations of the system described by Eqs. (3.9) and (3.10) (Nerenberg *et al.*, 1980).

The limitations of the simple phenomenological model discussed above are obvious. It would be of interest to construct a model in which the interaction strength depends on frequency, temperature, distance, and material. The experimental evidence for such dependence is strong. It has been found that pairs of microbridges in tin could phase lock and radiate coherently over a longer interbridge distance than similar bridges in indium (12 μm as compared to 4 μm) and that the locking strength was strongly temperature dependent—see Figs. 13 and 14 (Lindelof and Bindslev Hansen, 1977b). Moreover, the voltage- and phase-locking between tin and indium microbridges has been found to vanish at voltages (frequencies) higher than about 30—40 μV ($\nu_J \approx 15$—20 GHz) (Jillie *et al.*, 1977b).

Experiments on pairs of closely spaced *aluminium* microbridges have so far been unsuccessful in showing any of the static and dynamic interaction phenomena observed for similar systems in tin and indium (Daalmans *et al.*, 1977; Lindelof *et al.*, 1978). This is surprising since the inelastic relaxation time τ_E (and therefore also Λ_{Q^*}) is much longer in aluminium than in the two other superconductors. Recently Stuivinga *et al.* (1983) have measured Λ_{Q^*} in a one-dimensional aluminium strip to be about 25 μm at $T=0.99T_c$.

One of the most interesting observations made by Jillie *et al.* (1977b) in their system of two thin-film indium microbridges ($d \approx 2$ μm), was the strong temperature and voltage dependence they found for the strength of the voltage-pulling and -locking as measured by the maximum change in the dynamic resistance $\Delta(dV/dI)$. The interaction was generally strongest just below T_c and fell off rapidly with decreasing temperature. Already at $T=0.98T_c$ full voltage locking (opposed-biased) could no longer be obtained. At $T=0.9T_c$ the interaction could just still be observed. For constant temperature, the strength exhibited an oscillatory behavior (and at the same time a general falloff) as a function of increasing voltage, as shown in Fig. 15(a). The voltages corresponding to the extrema values increased systematically with decreasing temperature like the energy gap (or perhaps slightly quicker), i.e., approximately as $(1-t)^{0.5}$. Furthermore, the voltages corresponding to the first four extrema seemed to fall in a series with the ratios $1{:}2{:}\frac{9}{4}{:}\frac{5}{2}$, as shown in Fig. 15(b) (Jillie *et al.*, 1980).

In the following we shall discuss two different quasiparticle interaction mechanisms that could give rise to voltage locking. This discussion will be concerned with collective modes for the electronic system in superconductors.

(i) An asymmetrical, energy-selective quasiparticle interaction mechanism. This coupling mechanism only involves quasiparticles within a narrow range of energies. The idea is that the quasiparticle diffusion currents can perturb each other at energies around the gap edge singularity (Lindelof and Bindslev Hansen, 1977,1981). It assumes that the energy distribution of the quasiparticles diffusing through the interlink region is not a smooth function but has a sharp maximum at the energy corresponding to the gap singularity in the superconductors beyond the weak links. This idea is illustrated in Fig. 16. The voltage bias V_2 across the weak link shown to the right is constant. The three pictures display the quasiparticle distribution in the semiconductor picture for three different voltages V_1 across the left bridge. From top to bottom, this corresponds to the series situation $V_1=0$ and the opposed-biased configuration. The small peaks in the distribution correspond to the injection from the gap singularity through a weak link to another superconductor. Only the opposed-biased case will show voltage locking. The locking comes about because the diffusion current from bridge 1 which is injected through weak link no. 2 (compare with Fig. 8) will be particularly large when the gap singularity of the right superconductor is on the same level as the peak in the injected distribution in the middle superconductor. This interaction has been observed in experiments with two tunnel junctions back to back (Kaplan *et al.*, 1977).

We note that the asymmetry inherent in this interaction has the same "sign" as the one observed by Jillie *et al.* (1977b). This again was the same as the sign for the *antisymmetrical* dc interaction due to the effect on the critical currents of the injected quasiparticle currents.

Forming a linear combination of the wave functions for the degenerate states of electronlike and holelike character at the energy E and the wave numbers k_4 and $-k_2$, as shown on the quasiparticle dispersion curves in Fig. 17, we get

$$\psi = \tfrac{1}{2}\psi(-k_2) + \tfrac{1}{2}\psi(k_4) \ . \tag{3.11}$$

If these wave functions have plane-wave character, we have

$$\psi = \cos k_F x e^{iqx} e^{-i(E-\Delta)t/\hbar}, \tag{3.12}$$

where $q = k_F - k_2 = k_4 - k_F$. The resulting de Broglie wavelength $\lambda = 2\pi/q$ for quasiparticles in the injected peak will be much longer than for electrons in a normal metal. An excitation energy

$$E = eV + \Delta \tag{3.13}$$

will give a wave vector which in the free-electron approximation is determined by

$$\hbar v_F q = (E^2 - \Delta^2)^{1/2} \approx \sqrt{2eV\Delta}, \tag{3.14}$$

for $q/k_F \ll 1$ and $V \ll \Delta/e$. The relation (3.14) predicts a decreasing wavelength both with increasing voltage and increasing gap (decreasing temperature). For indium at $T = 0.97T_c$ we get $\lambda = 2\pi/q = 400\ \mu\text{m/V}^{1/2}$, where V is measured in μV. Hence for $T = 0.97T_c$ and $V = 20\ \mu$V, $\lambda = 90\ \mu$m. The characteristic decay length of the injected peak in the spectrum is much shorter. If the interbridge region can be considered to be an isolated piece of superconductor, this length will be $\Lambda_E = (D\tau_E)^{1/2}$. This is an upper limit. Normally, diffusion will wash the peak out quicker than that. In indium $\Lambda_E \approx 2\ \mu$m. Consequently,

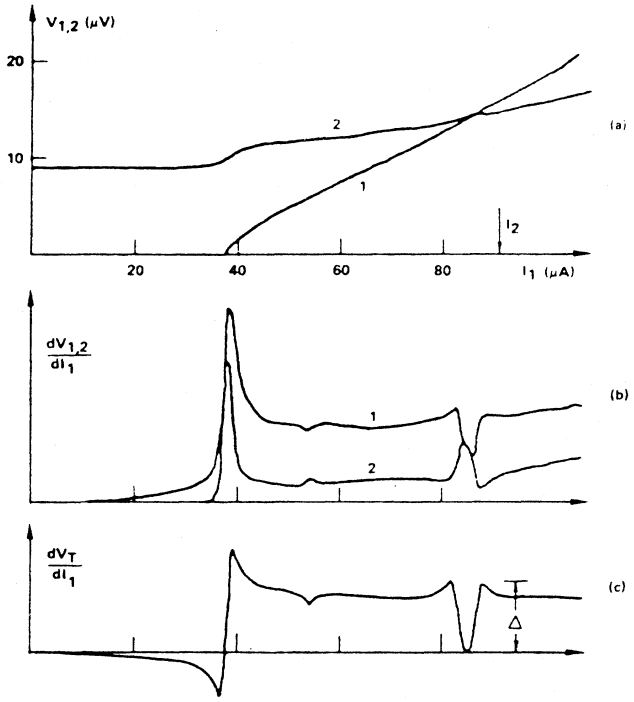

FIG. 10. Experimental results (a), (b), and (c) for an opposed-biased pair of indium microbridges 2 μm apart showing voltage locking. (a) $V_1 - I_1$ and $V_2 - I_1$ curves with I_2 held constant (91 μA) and I_1 swept; (b) the differential resistance of the two curves shown in (a); and (c) the total differential resistance $dV_T/dI_1 = dV_1/dI_1 - dV_2/dI_1$. During voltage locking $dV_T/dI_1 = 0$. In the locking region $\Delta(dV_T/dI_1)$ is a measure of the strength of the interaction (Jillie *et al.*, 1980).

the mode is heavily damped. It might be a relevant mode for a pair of aluminium bridges with a restricted geometry between the bridges, since for Al $\Lambda_E = 60\ \mu$m and $\lambda = 800\ \mu\text{m/V}^{1/2}$ (V in μV) and therefore $\Lambda_E \approx \lambda/3$ for $V = 20\ \mu$V.

(ii) Diffusing or propagating quasiparticle charge imbalance. The second quasiparticle coupling mechanism involves the dynamics of the charge imbalance generated in and around Josephson weak links. The quasiparticle potential μ_{qp} decays over a length which at low frequencies is the charge imbalance diffusion length, $\Lambda_{Q^*} = (D\tau_{Q^*})^{1/2}$. When the frequency exceeds $1/\tau_E$, the inverse inelastic relaxation time, the length becomes shorter due to a skin-depth effect, $\Lambda_{ac} = \sqrt{2D/\omega} < \Lambda_{Q^*}$. At even higher frequencies, when $\omega > 1/\tau_J = (1/\tau)(n_s/n)$ (but still $\omega < 2\Delta/\hbar$ to avoid the anomalous absorption above the gap frequency), a charge imbalance collective mode with a soundlike spectrum may propagate through the superconductor, as observed by Carlson *et al.* (1975,1976) and treated theoretically in the clean limit by Artemenko *et al.* (1979) (τ_J is the supercurrent response time).

Based on the description of the charge imbalance within the generalized two-fluid model of Pethick *et al.* (1979), Kadin *et al.* (1980) derived the following charge imbalance wave equation, valid for $\Delta/k_BT < 1$ (see also Lindelof, 1978)

$$\Lambda_{Q^*}^2 \nabla^2 Q^* = \tau_J \tau_E \frac{d^2Q^*}{dt^2} + (\tau_J + \tau_E)\frac{dQ^*}{dt} + Q^* . \tag{3.15}$$

For $\omega^2 \tau_J \tau_E \gg \omega(\tau_J + \tau_E)$, i.e., for $\omega \gg \tau_J^{-1}, \tau_E^{-1}$, this equation describes propagating charge imbalance waves with velocity $v = \Lambda_{Q^*}(\tau_J\tau_E)^{1/2}$. In the dirty limit $v = \sqrt{2D\Delta/\hbar} \approx 0.6 v_F (l/\xi_0)^{1/2}(1-t)^{1/4}$. In this limit the same propagating collective mode has been treated by Schmid and Schön (1975,1981) (within a different framework[5]). The dispersion relation is linear $\omega = vq$. It consists of a countermotion of normal fluid and superfluid which ensures charge neutrality and therefore screens the Coulomb interaction.

Kadin *et al.* (1980) provided new insight into the nature of such propagating charge imbalance waves by demonstrating that, for the case of a one-dimensional nonequilibrium superconductor close to T_c, they are completely analogous to electromagnetic waves on a transmission line as described by the classic telegraph equation. It should be noted that, in general, such a charge-imbalance wave is heavily damped by the dissipative processes involved in the oscillation of the normal fluid. It exists only close to T_c; see Fig. 18. At high frequencies, the ac decay length $\Lambda_{ac} = 2\Lambda_{Q^*}(\tau_J\tau_E)^{1/2}/(\tau_J + \tau_E)$ is only of the order of the coherence length ξ.

Imagine now two weak links placed close together and both in the voltage-sustaining state. Close to T_c and at appropriately high frequencies, the ac Josephson oscilla-

[5]It is called the transverse mode in the terminology of Schmid and Schön.

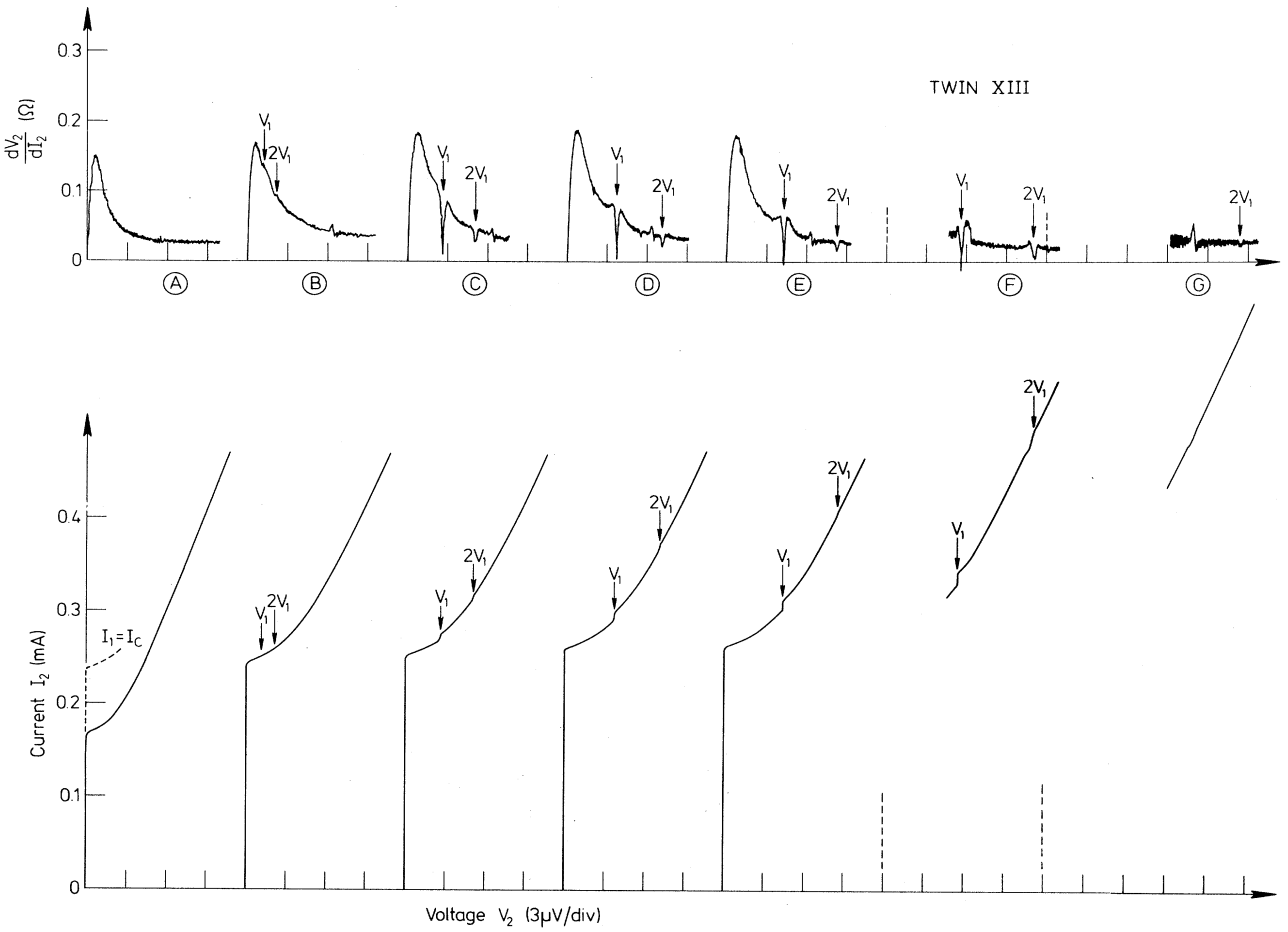

FIG. 11. Experimental results showing voltage locking between two indium microbridges placed 1.8 μm apart. I-V and dI/dV vs V curves are shown for bridge 2 with bridge 1 biased at six different fixed currents (in A $I_1=0$). The phase-locked steps are seen at $V_2=V_1$ and also at $V_2=2V_1$. The critical current of bridge 2 is enhanced already for $I_1<I_{c1}$ (see broken I-V curve for $I_1=I_{c1}$), an observation that cannot be explained by the interaction models discussed here (Lindelof *et al.*, 1977).

tions in one weak link will generate outgoing charge imbalance waves that will interfere with the same oscillations in and around the other weak link. The oscillations in the two weak links will lock together due to this oscillating potential. Mutually induced steps in the I-V curves and the generation of coherent Josephson radiation would be the result.

The outgoing charge imbalance wave generated in a weak link is reflected in the other weak link and comes back to its source with a phase that depends on the frequency, the distance between the weak links, and the phase shift in the other weak link. The amplitude of the wave will naturally die out over the characteristic length Λ_{ac}. Note that even at lower frequencies where the charge imbalance waves cannot propagate, a phase shift will still occur within the skin depth. Figure 19 illustrates qualitatively the amplitude of the reflected wave that comes back to its origin after having undergone reflection in the other weak link (Lindelof and Bindslev Hansen, 1977b). Constructive or destructive interference will be observed depending on the distance between the weak links as shown. This effect is, of course, reciprocal. The wave train from one weak link may injection-lock the oscillation in the other weak link, provided the amplitude exceeds the noise level. If that happens, the reflected wave will normally be both amplified and phase shifted by the injection-locking process. To treat this charge-imbalance-wave coupling quantitatively, including the spatial resonance phenomena connected with the "Fabry-Perot resonator" formed by the two weak links, Kadin *et al.* (1980) suggested the

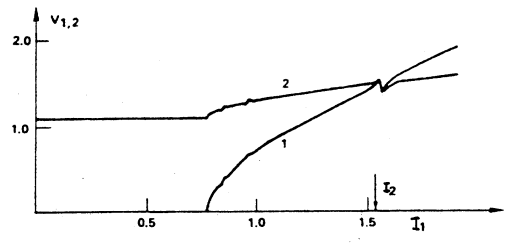

FIG. 12. Numerical simulation of the quasiparticle interaction, Eqs. (3.9) and (3.10). The measured values for the coupled bridges in Fig. 10 ($\alpha_1=\alpha_2=0.21$) have been used (Jillie *et al.*, 1980).

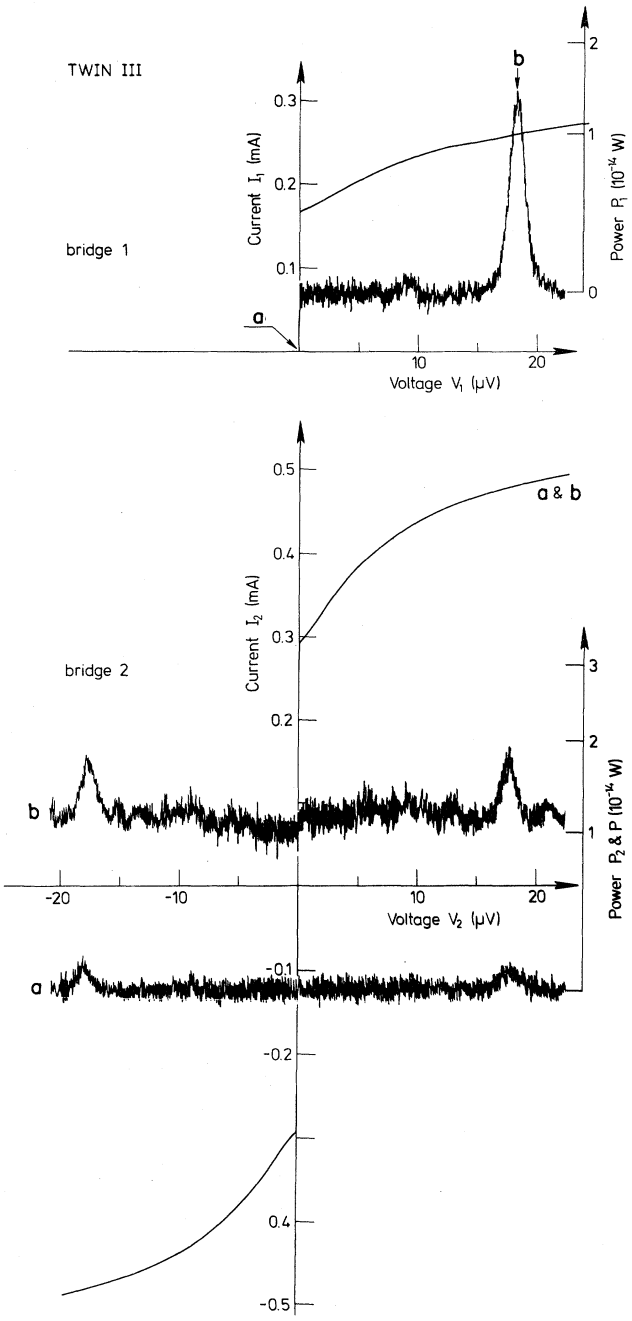

FIG. 13. Example of observation of coherent (in-phase) microwave radiation from a pair of tin thin-film microbridges placed close together in the same superconducting medium ($d=12$ μm). The upper figure shows I, and the microwave power at 8.7 GHz vs V_1. The lower figure shows the same for bridge 2 but with bridge 1 biased both at a and b. The interaction is symmetrical in the bias current directions (Lindelof *et al.*, 1977).

transmission line equivalent circuit shown in Fig. 20. Blackburn (1983) carried out numerical simulations of this one-dimensional system and found strong phase-locking effects when the distance was less than a few

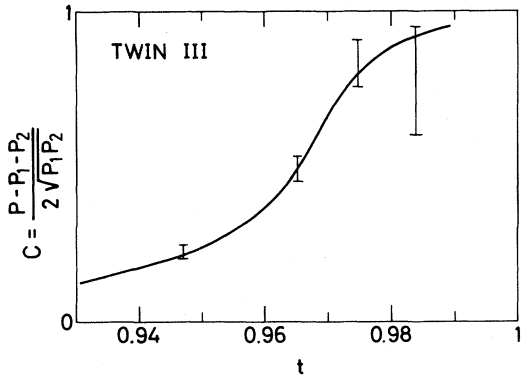

FIG. 14. Observed temperature dependence for the broadband high-frequency interaction between weak links placed close together. The (in-phase) coherence ratio C is plotted vs the reduced temperature $t=T/T_c$ for the same pair of tin bridges as in Fig. 13 (Lindelof *et al.*, 1977).

times Λ_{Q^*}. An example of the calculated temporal and spatial variation of the quasiparticle potential μ_{qp} for $d=\Lambda_{Q^*}$ is reproduced in Fig. 21. The low-Q spatial resonances expected in the system could not be seen in these numerical simulations. Amatuni *et al.* (1982) have found analytical solutions for the charge-imbalance-wave coupling between two planar (two-dimensional) weak links for $I_cR_N < V \ll \Delta$. They also predicted weak spatial resonances in the coupled strength. In experiments with coupling between tin microbridges 3 to 30 μm apart they did observe the predicted distance-dependent phase-locking effects but only when the two series-connected junctions were synchronized by an external microwave source. It is not clear to what extent this external perturbation masked the intrinsic coupling effect.

In our opinion, clear, quantitative, experimental evidence for the existence of charge imbalance waves near a Josephson weak link is still lacking. Resonant self-detection of such waves in and around a single weak link may have been observed by Kadin *et al.* (1981), though the temperature dependence of the observed mode velocity seemed to deviate from the theoretical prediction [$v \propto (1-t)^{1/4}$].

IV. LONG-RANGE INTERACTIONS

A. General principles

A long-range dynamic coupling between Josephson weak links may be established by means of suitable external circuitry, e.g., a common resistive or superconducting shunt, or a common transmission line or resonator. In this case the spacing between the weak links may naturally be much larger than the characteristic length scales of the superconducting medium. The nonequilibrium effects (including heating) that may give rise to the short-range interactions can therefore be made negligibly small. This can be a desirable property in practical applications of systems of coupled weak links, although for other reasons

comparatively closely packed arrays of junctions are often needed.[6]

In order to describe long-range interactions the RSJ model will almost always give a fully adequate description of the properties of the Josephson elements.

As mentioned previously, the impedance of a weak link is, in general, low compared with the characteristic impedance of conventional microwave transmission lines $Z_0 \approx 100\ \Omega$. Therefore, the oscillating potential across a Josephson weak link will be able to drive only an extremely weak ac current through the outer circuit having this large impedance. This impedance mismatch problem must be solved if we want to couple a decent amount of power out of the weak link or if we want to establish a long-range coupling between two or more weak links.

Two series-connected weak links may be coupled simply by providing them with a common low-impedance shunt that allows a circulating ac current to be set up by the oscillating potentials across the two links; see Fig. 22(a).

Connecting two weak links in parallel [Fig. 22(b)], of course, also provides a path for a circulating coupling current. If the loop is made superconducting, we simply have a dc-SQUID, a two-junction quantum interferometer.

B. Two weak-links series coupled through a common shunt

The advantage of using an external shunt loop is the wide band over which coupling can be achieved. For nearly identical junctions with a common shunt, the locking range $\Delta\omega_{\text{lock}}$ is to first order ($Z_s \gg R$) proportional to the shunt loop admittance $Y_s(\omega)$, where $1/Z_s = (1/R_s)+iY_s$ (Likharev *et al.*, 1981, and Kuzmin *et al.*, 1982). The reactance of the shunt introduces an electromagnetic phase shift $\Delta\theta$ between the junctions. In the case of two series-connected weak links with an R-L shunt loop we have

$$\Delta\theta = \tan^{-1}\left[\frac{\omega L}{R_{N1}+R_{N2}+R_s}\right]. \tag{4.1}$$

For a pair of identical weak links coupled by an R-L loop, the current locking range ΔI_{lock} becomes maximum for $\Delta\theta=\pi/4$, i.e., for $\omega L = R_{N1}+R_{N2}+R_s$ (Jain *et al.*, 1979; Likharev *et al.*, 1981). This phase difference ensures that both junctions are biased close to the centers of their mutually induced phase-locked "steps" in the I-V characteristics, thus providing a wide range for change in the common bias current before going out of lock. $\Delta\theta=\pi/2$ would correspond to the centers of the steps,

[6]The close packing may be necessary in order (1) to reduce the self-inductance of the connecting pads between the weak links (to increase the upper frequency limit) and (2) to accommodate the array within a small fraction of a wavelength, so that all junctions are located in the same phase plane.

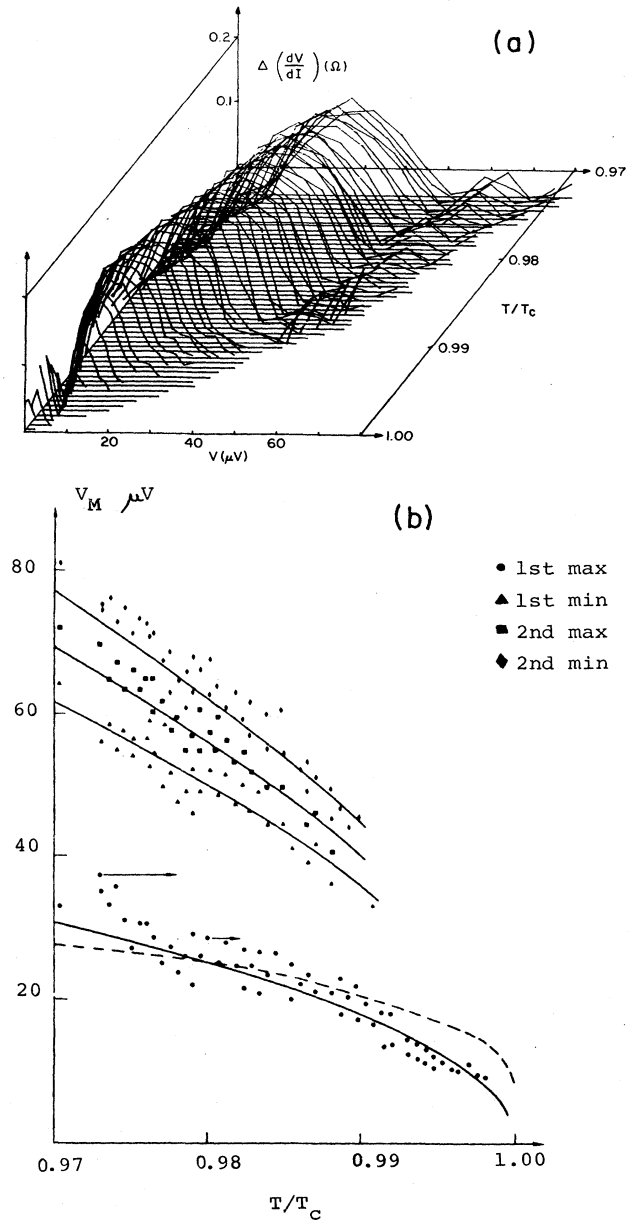

FIG. 15. (a) Measured variation of the voltage-locking strength $\Delta(dV_T/dI)$ with temperature and voltage; see Fig. 10(c). Full locking (i.e., $dV_T/dI=0$) is observed on the main peak in the region from $t=T/T_c=0.998$ to $t=0.980$ and also near zero voltage in the region very close to T_c. These data were obtained for a pair of planar indium microbridges (film thickness equal to 100 nm) in the opposed-biased current configuration. As the temperature is lowered further, $\Delta(dV_T/dI)$ becomes smaller and finally disappears at $t\sim 0.90$ (Jillie *et al.*, 1980). (b) Measured voltage positions V_M of the minima and maxima of the locking strength $\Delta(dV_T/dI)$ [from (a)] plotted as a function of the reduced temperature $t=T/T_c$. The solid lines are proportional to $(1-t)^{1/2}$; the dotted line is proportional to $(1-t)^{1/4}$. The two arrowed points indicate the estimated maximum effect due to heating. The solid curves for the first minimum, second maximum, and second minimum are, respectively 2, $\frac{9}{4}$, and $\frac{5}{2}$ times the curve for the first maximum, which may be related to a resonance phenomenon (Jillie *et al.*, 1980).

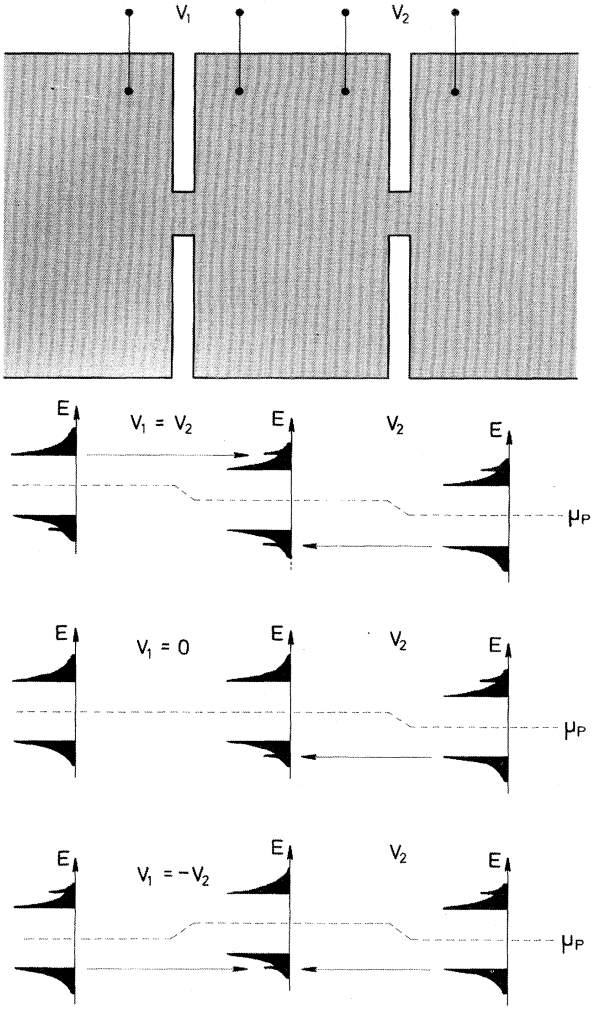

FIG. 16. Qualitative illustration of the asymmetrical quasiparticle dc voltage-locking mechanism. The superconducting film with the two closely spaced microbridges are shown at the top. Below that and with the same x axis, the variation of the pair potential μ_p through the system is shown for three different bias situations (V_2 is constant): $V_1=V_2$ (series), $V_1=0$, and $V_1=-V_2$ (opposed biased). The quasiparticle distribution in the three regions with the injected peaks due to the diffusive currents is also shown. The dc voltage locking occurs only for the opposed-biased current configuration (lowest picture), as discussed in the text (Lindelof *et al.*, 1981).

but that would require $L\rightarrow\infty$, and no coupling current would flow. The characteristic frequency of the circuit is

$$\nu=\frac{R_{N1}+R_{N2}+R_s}{2\pi L}\ , \tag{4.2}$$

which sets the frequency scale for the coupling bandwidth. This frequency is typically of the order of a few GHz. For a capacitive shunt loop the two series-connected junction will oscillate in antiphase at the middle of the step. Likharev *et al.* (1981) and Kuzmin *et al.* (1982) have calculated the I-V curves in the locking region for series- and for parallel-connected junctions with inductive or capacitive shunt loops. They showed that for

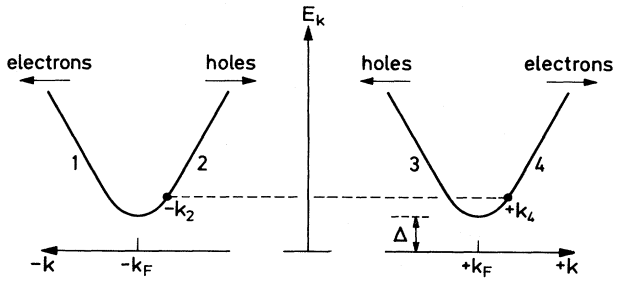

FIG. 17. Dispersion curves around the Fermi level for the quasi particles in a 1D superconductor.

applications the optimal configuration is a series array with an R-L shunt loop that yields in-phase oscillations at the center of the phase-locked region. In order to avoid impedance discontinuities at the ends of the array they proposed a ring-formed series array (i.e., establishing a periodic boundary condition for the array system).

Systems with capacitive coupling between weak links have also been treated theoretically by Giovannini *et al.* (1978). Zhang *et al.* (1983) have recently investigated a bistable flip-flop circuit with two weak links coupled through an R-C shunt.

Investigations of long-range coupling via R-L shunts have been reported by Varmazis *et al.* (1978), Sandell *et al.* (1979a), Jain, Mankiewich, and Lukens (1980), Jain, Kadin *et al.* (1980), and Jain *et al.* (1982a,1982b).

These experimental results obtained for the R-L shunt-loop coupling between two microbridges in many ways resembled the results described above for proximity-coupled weak links, e.g., two 0.1-Ω indium bridges, 12 μm apart and shunted by a 0.2-Ω gold resistor placed 4 μm from the weak links, exhibited strong dc voltage-pulling and -locking effects when both junctions were biased around the same voltage.[7] A few differences in the detailed behavior of the two systems were, however, also seen. The most important distinction from the proximity-coupled case was the absence of any strong temperature or voltage dependence of the coupling strength.

Phase locking was also observed for two resistively coupled bridges, as proved by the detection of (in-phase) coherent radiation. Here the only dissimilarity with the proximity-coupled case lay in the shape of the coherent radiation peak, whose linewidth was 50% and 150% of that of a single bridge for the series and opposed-biased configurations, respectively, Sandell *et al.* (1979a). A much stronger linewidth-narrowing effect (10%) for two phase-locked proximity-coupled microbridges was reported by Varmazis *et al.* (1978).

For both bias configurations, Sandell *et al.* (1979a)

[7]Phase coherence was observed up to 18 GHz ($\approx$40 μV)—at temperatures close to T_c limited by the characteristic frequency $\nu=R/2\pi L\approx 6$ GHz of the coupling loop; at lower temperatures limited and eventually destroyed by heating effects in the thin-film planar bridges.

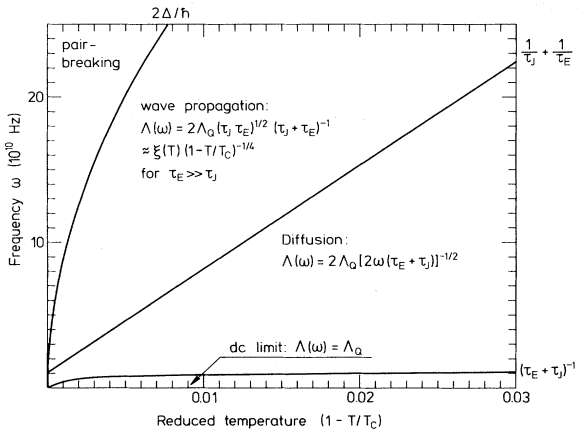

FIG. 18. Different regimes of solutions to the charge-imbalance wave equation shown in a frequency-temperature diagram. The charge-imbalance relaxation time τ_{Q^*} and the current relaxation time τ_J both depend on temperature. At high frequencies pair breaking will dominate and the description breaks down. Furthermore, the description is valid only close to T_c where $\Delta/k_B T_c \ll 1$ (Lindelof, 1981).

were able to explain the relative magnitude of the observed linewidth $\Delta\nu$ on the basis of the measured dynamic resistance R_d (neglecting the noise in the shunt), by using $\Delta\nu \propto R_d^2$ (Likharev *et al.*, 1972).

Theoretically, the RSJ model used for the two resistively shunted junctions shown in Fig. 22(c) yields (Nerenberg *et al.*, 1980)

$$I_1 = I_{c1}\sin\phi_1 \pm \alpha_2(I_2 - I_{c2}\sin\phi_2) + \frac{1}{R_{N1}||(R_{N2}+R_s)}V_1 , \tag{4.3}$$

$$I_2 = I_{c2}\sin\phi_2 \pm \alpha_1(I_1 - I_{c1}\sin\phi_1) + \frac{1}{R_{N2}||(R_{N1}+R_s)}V_2 , \tag{4.4}$$

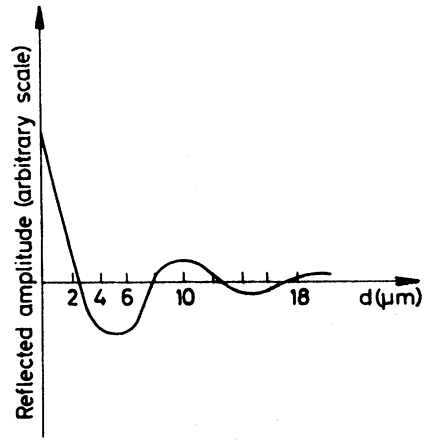

FIG. 19. Qualitative picture of the reflected amplitude of the Josephson oscillation from bridge 1 via bridge 2 back onto itself (if there is no phase shift at bridge 2). Such a "Fabry-Perot resonance" may be connected with both of the proposed "low-frequency" quasiparticle modes (Lindelof *et al.*, 1977).

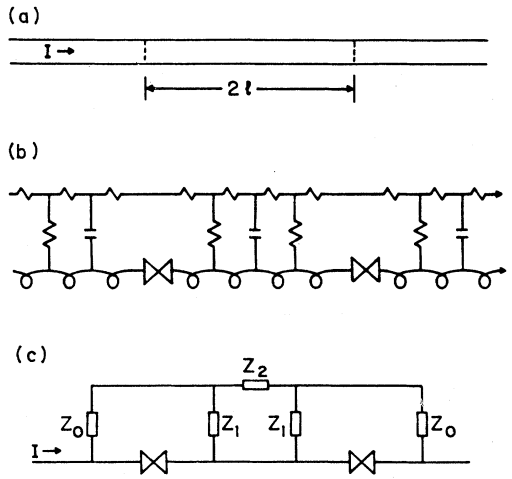

FIG. 20. Equivalent circuit diagrams for two 1D weak links (phase-slip centers) coupled through a quasiparticle charge-imbalance wave (Kadin *et al.*, 1980). (a) Superconducting strip with two weak spots (indicated by dashed lines) which act to nucleate the phase-slip centers. (b) Transmission line equivalent of (a). (c) Equivalent circuit diagram with lumped impedance elements. This circuit has been analyzed by Kadin (1979).

where

$$\alpha_1 = \frac{R_{N1}}{R_{N1}+R_s} , \tag{4.5}$$

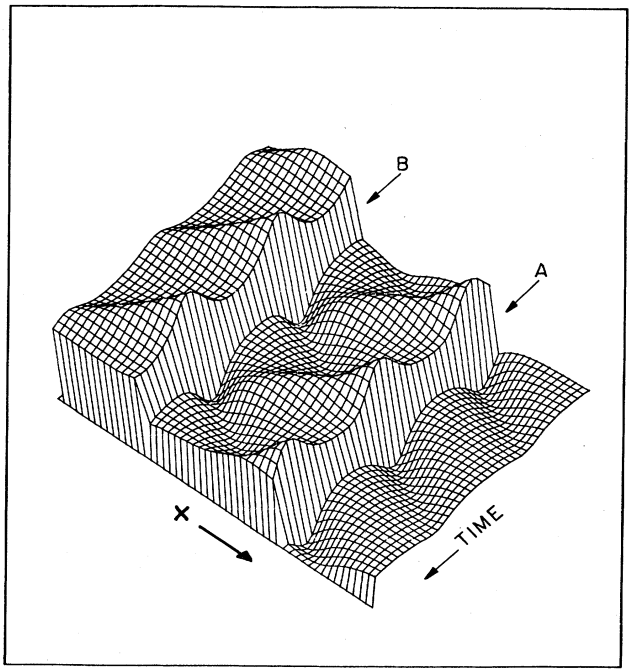

FIG. 21. The ac quasiparticle interaction: results of a digital computer simulation (Blackburn, 1983). Here is reproduced part of the quasiparticle potential surface $\mu_{qp}(x,t)$ around two 1D phase-slip centers (PSC), here called A and B, placed Λ_{Q^*} apart. The interference pattern of the charge-imbalance waves traveling outwards from the two PSC's is clearly seen.

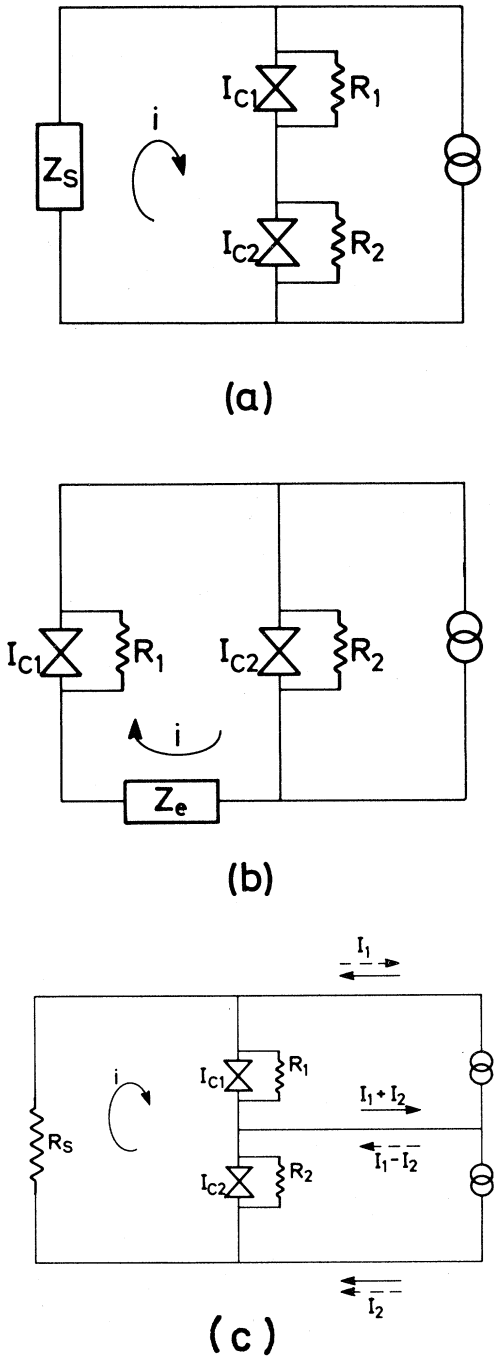

FIG. 22. (a) Two series-connected weak links with a common shunt Z_s. (b) Two parallel-connected weak links. If Z_e is purely inductive, a dc SQUID (superconducting quantum interference device) is formed. (c) Equivalent circuit diagram for two RSJ-model weak links coupled by an external resistive shunt and biased by two independent current sources. The two current configurations are shown (opposed biased, solid lines; series biased, broken lines).

$$\alpha_2=\frac{R_{N2}}{R_{N2}+R_s} , \tag{4.6}$$

and where the following notation has been used:

$$x||y=\left[\frac{1}{x}+\frac{1}{y}\right]^{-1} . \tag{4.7}$$

For the unperturbed case ($R_s\rightarrow\infty$) Eqs. (4.3) and (4.4), of course, reduce to

$$I_1=I_{c1}\sin\phi_1+\frac{V_1}{R_{N1}} , \tag{4.8}$$

$$I_2=I_{c2}\sin\phi_2+\frac{V_2}{R_{N2}} . \tag{4.9}$$

The following simple description of the effect of the resistive-coupling shunt on the microbridges in the non-stationary state may now be given: a fraction α_2 of the unperturbed normal current through bridge 2 is running through bridge 1 (the direction is determined by the current configuration), and the voltage across bridge 1 is loaded by a resistance which is R_{N1} in parallel with $R_{N2}+R_s$—and similarly for bridge 2. This description in terms of extra ("injected") normal currents is the same as that which was used in the case of direct proximity coupling through the oscillating quasiparticle potential; see Sec. III.C.3.

Analyzing the similarities in the experimental results on bridges coupled by a resistive shunt and on proximity-coupled bridges, and deriving the above-mentioned isomorphic formulas (to first order) for the two cases, Jillie *et al.* (1980) were led to suggest that a *common mechanism* might be responsible for coupling in both resistively shunted and closely spaced microbridge pairs. There are, however, physically significant differences in the observations reported for the two systems. First and foremost is the temperature dependence of the interaction strength, but also in the voltage dependence and in the linewidth of the coherent radiation, not to speak of the material dependence.

The connection between the observation of coherent radiation from weak links and the observation of dc voltage locking and pulling was addressed by Nerenberg *et al.* (1980) and by Deakin *et al.* (1982,1983). Solving Eqs. (4.3) and (4.4) both by a perturbation-theory approach and by numerical integration, they predicted the shape and the width of the dc voltage-locking intervals. They found, moreover, that just outside the locking regions phase coherence between the Josephson oscillations still prevailed, only interrupted regularly by rapid phase slips of 2π. This behavior offered a natural explanation of the observation of coherent radiation from two bridges whose dc voltages differed by as much as a few percent[8] (Lin-

[8]Note that $\langle V_1\rangle\neq\langle V_2\rangle$ implies only $(\hbar/2e)\langle\dot{\phi}_1\rangle\neq(\hbar/2e)\langle\dot{\phi}_2\rangle$. Therefore, since it is only the dc components of $\dot{\phi}_1$ and $\dot{\phi}_2$ that differ, it is still possible to have the (average) phase difference $\phi_1-\phi_2$ stable, e.g., around 0 (modulo 2π), over many Josephson periods, to have it then quickly slip by 2π, to have it be stable again over many cycles, to have it slip again, etc., so that $\langle\dot{\phi}_1-\dot{\phi}_2\rangle\neq0$ is fulfilled, while the phase coherence is virtually not affected.

delof and Bindslev Hansen, 1977; Varmazis *et al.*, 1978). The calculated voltage range over which coherent radiation should be observed exceeded by far the observed range (Deakin *et al.*, 1983). The effect of noise was, however, not included in these calculations. The stability of the phase-locked state of two Josephson oscillators in the presence of noise has been analyzed by Ambegaokar *et al.* (1981) and by Jillie (1981). Recently, Jain *et al.* (1982a,1982b) have shown experimentally that two weak links close to phase lock behave like one weak link biased at a voltage corresponding to the difference between the voltages of the two weak links (in the same way as the properties around a microwave-induced step closely resemble the properties close to the supercurrent).

C. SQUID coupling

1. Single two-junction SQUID

As said previously, the two-junction SQUID may be viewed as a pair of junctions coupled through a purely inductive shunt L; see Fig. 23. Investigations of the high-frequency behavior of dc SQUID's by measuring the radiated microwave power have been carried out by a number of groups [Silver *et al.* (1967); de Bruyn Ouboter *et al.* (1970) and references therein; Sandell *et al.* (1979b); Bindslev Hansen (1982)].

The quantization condition for the magnetic flux linking the loop leads to a flux-modulated phase shift, $\Delta\phi=\phi_1-\phi_2$, between the two Josephson oscillators

$$2\pi n=\phi_1-\phi_2+\frac{2\pi}{\Phi_0}\Phi$$
$$=\phi_1-\phi_2+\frac{2\pi}{\Phi_0}(\Phi_{\rm ext}+Li_{\rm circ})\,, \tag{4.10}$$

where $i_{\rm circ}=\frac{1}{2}(I_1-I_2)$ is the circulating current in the ring, $\Phi_{\rm ext}$ is the externally applied flux, Φ is the total flux linking the ring, n is an integer, and $\Phi_0=h/2e$ is the flux quantum ($\Phi_0=2.07\times10^{-15}$ V s).

The calculated periodic variation with $\Phi_{\rm ext}$ of the maximum zero-voltage current $I_{\rm max}$ and of the phase difference $\Delta\phi=\phi_1-\phi_2$ is shown in Fig. 24. For $\Phi_{\rm ext}=n\Phi_0$ the difference is zero (in phase), whereas for $\Phi_{\rm ext}=(n+\frac{1}{2})\Phi_0$ it is π (antiphase).

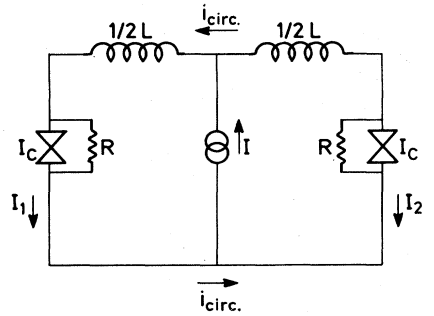

FIG. 23. Equivalent circuit diagram for a symmetrically biased dc SQUID. For simplicity the junction parameters are assumed to be identical.

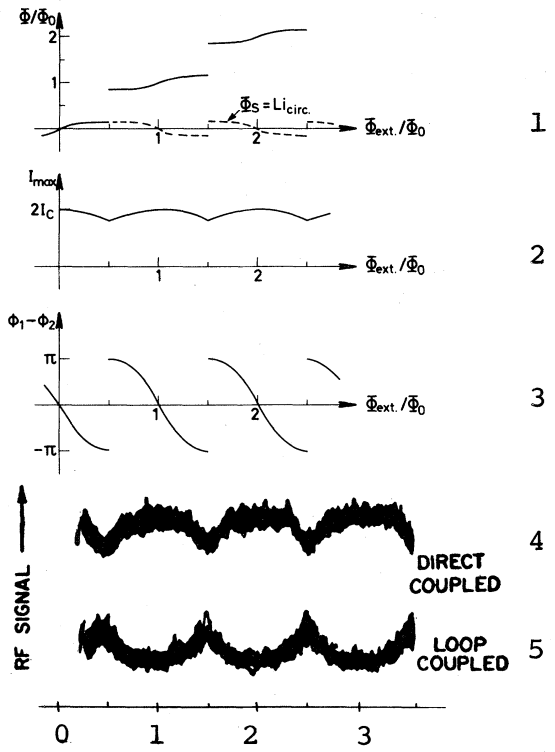

FIG. 24. Parameters describing the symmetrical dc SQUID (Fig. 23) plotted as a function of the applied magnetic flux. The *upper three* plots are *theoretical* curves. From the top: (1) total magnetic flux linking the SQUID loop (solid line) and self-induced flux, $Li_{\rm circ}$ (broken line) (taken from de Bruyn Ouboter and De Waele, 1970); (2) maximum zero-voltage current; (3) the difference of phases across the two junctions. The *lower two* curves are *experimental* traces (Silver *et al.*, 1967) showing the rf amplitude measured at 30 MHz; (4) rf detector symmetrically coupled to the SQUID across the current source (see Fig. 23); and (5) rf detector antisymmetrically connected to the SQUID (loop coupled).

There are essentially two orthogonal coupling schemes for probing the ac voltage amplitude across the dc SQUID: by measuring directly (symmetrically) across the current source or by inductive coupling to the oscillating voltage across the two $L/2$ inductances in series (see Fig. 23). Silver *et al.* (1967) coupled in both ways to their niobium double-contact SQUID and observed the periodic variation of the rf amplitude at 30 MHz shown in Fig. 24. Thus what we see here is the dynamic interference of two quantum oscillators that run at the same frequency and with constant rf amplitudes while their phase difference varies periodically with the applied flux, i.e., a flux-modulated rf generator.

As before, the bandwidth for the rf currents in the SQUID loop has an upper rolloff frequency determined by the R/L ratio:

$$\nu_{\rm rolloff}=\frac{2R_N}{2\pi L}\,. \tag{4.11}$$

2. Inductive coupling between SQUID's

SQUID's placed close together may couple dynamically through their mutual inductance (Bindslev Hansen *et al.*, 1981; Chi *et al.*, 1981). In the voltage-sustaining state high-frequency currents are set up in the multijunction-SQUID loops by the ac Josephson effects in the junctions. Via the mutual inductance, these currents modulate the flux through the adjacent SQUID's, and thereby modulate their voltages. The ac Josephson oscillations in the SQUID junctions may as a result lock together. The strength of the locking is dependent on the fluxoid state of the SQUID's. Coherent behavior of two broadband oscillators like the Josephson weak links requires a mutual interaction, i.e., a flow of "amplitude and phase information" in both directions. It is therefore necessary that the fluxoid state of the SQUID's be such that each of them can induce *and* detect an ac voltage/current in the others. For coupled symmetrical dc SQUID's it turns out that the locking strength becomes maximum for $\Phi \approx (n \pm \frac{1}{3})\Phi_0$ (Bindslev Hansen, 1982).

In wide Josephson junctions ($w > \lambda$, e.g., proximity-effect bridges) the current density across the junction will be nonuniform. For junctions of this kind, closely spaced in series, the circulating currents connected with the presence of one or more flux quanta in the junctions may give rise to an inductive coupling similar to the one just described for coupled SQUID's (Imry *et al.*, 1978; Frank *et al.*, 1978; Mineev *et al.*, 1981; Weiss-Parmeggiani, 1982).

D. Coupling via a low-impedance transmission line

Up to now we have considered only simple circuits that can be described by lumped passive circuit elements. We will now treat high-frequency coupling schemes that are most appropriately characterized by distributed circuit elements, that is, microwave transmission lines and cavity resonators.

As already discussed, a long-range electromagnetic interaction between weak links requires a circuit of sufficiently low impedance, Z linking them together. Conventional microwave transmission lines in the form of wave guides and coaxial cables are not very useful in that respect. However, transmission lines of stripline, microstrip, or slotted line type [see Fig. 25(a)] can be designed to have a suitably low impedance. In addition, these transmission-line structures can be fabricated in the same thin film as the weak links; it is, in fact, in many cases essential that these thin-film low-impedance transmission lines be made from superconducting materials. If not, the surface losses are high and the signals are heavily damped. Figure 25(b) shows the characteristic impedance as a function of dimensions for these transmission-line structures. It is clear that in order to construct a transmission line with a Z at the 0.1-Ω level, the ratio between the width W of the line and thickness H of the dielectric layer has to be made very large ($W/H \gtrsim 200$). In practical microstrip design (with $W \simeq 1$ mm) this implies that an extremely thin dielectric layer is needed ($H \lesssim 5$ μm). Moreover, in order to minimize dispersion and dielectric losses, the solid dielectric may, with great advantage, be replaced by vacuum (or helium)—a so-called inverted microstrip configuration. Weak links would couple strongly and over a wide band via a microstrip transmission line which could also be made to include a tapered or stepped impedance-transformer section to match the outer circuit—at least over a restricted bandwidth; see Fig. 26. Impedance matching configurations

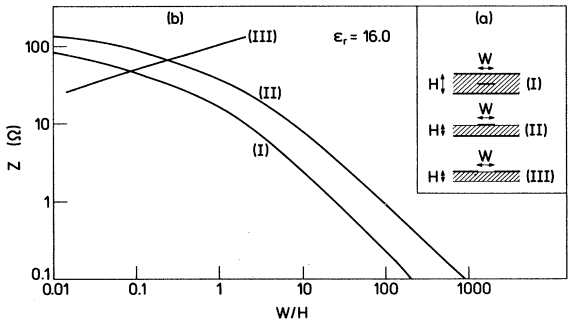

FIG. 25. (a) Inset: thin-film microwave transmission lines suited for coupling to and between Josephson thin-film devices: I, microstrip line (balanced microstrip), II, microstrip, and III, slot line. The hatched areas indicate dielectric material, the heavy lines metallic film. (b) The characteristic impedance Z of the three transmission line structures shown in (a) plotted vs the geometrical ratio W/H. W is the width of the strip (slot), and H is the thickness of the dielectric. Here Z vs W/H is plotted for a dielectric with $\epsilon_r = 16.0$. Z scales with $\epsilon_r^{-1/2}$ [for a recent textbook on these structures see Gupta *et al.* (1979)].

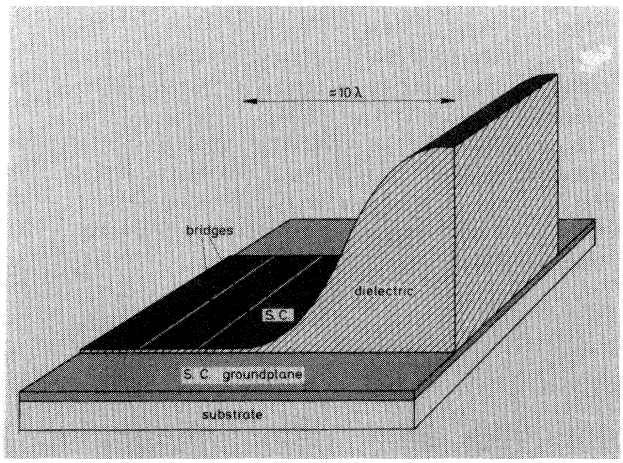

FIG. 26. Drawing showing *in principle* how to couple two Josephson weak links via a low-impedance microstrip transmission line with a large W/H ratio (see Fig. 25) and how to use a tapered impedance-transformer section of the microstrip to establish a good coupling to an external high-impedance transmission line. Since the width of the line should not exceed $\lambda/2$, the 10λ tapered section is considerably compressed in the drawing.

with a low impedance of the order of 1 Ω or less have been realized experimentally for coupling to a single junction at 35 GHz by Sørensen *et al.* (1981) and by Hohenwarter *et al.* (1981). There have not yet been any reports on similar systems including arrays of junctions.

E. Coupling via a resonator

Making the transmission line resonant, i.e., forming a cavity, and using that as the coupling medium may establish a strong coupling at the resonance frequency at the expense of a narrow bandwidth for the coupling. The case of a single Josephson weak link coupled to a series resonator has been studied by many groups. For a low-capacitance weak link, we can summarize the main characteristics of the complex nonlinear interaction between the Josephson junction and the series resonator as follows (Vystavkin *et al.*, 1974; Gubankov *et al.*, 1975; Krech *et al.*, 1979): (i) at resonance the impedance mismatch between the junction and the microwave circuit is reduced by a factor of Q, the loaded quality factor of the cavity; (ii) due to the regenerative interaction between the nonlinear junction and the cavity field the linewidth of the Josephson radiation is narrowed ("self-detection"); (iii) in the dc I-V characteristic a cavity-induced step appears, protruding downwards towards the low-current side of the I-V curve; and (iv) parametric generation of so-called "non-Josephson" radiation is observed at the resonance frequency $\nu_{\rm res}$ when the junction is biased just below the cavity-induced step, $\langle V\rangle \lesssim h\nu_{\rm res}/2e$. This radiation is emitted simultaneously with the Josephson radiation at the frequency $\nu_J = 2e\langle V\rangle/h$.

Let us now consider two weak links coupled to a common series resonance circuit and connected to two separate current sources. At resonance, the impedance of the series resonator is minimum and given by the real part, r, of the resonator impedance, thus providing an effective short circuit for the ac currents at the resonance frequency. Figure 27 shows the simplest possible equivalent circuit. If we again use the RSJ model for the

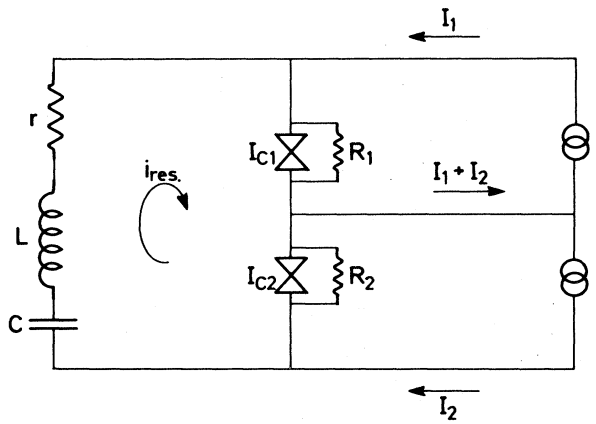

FIG. 27. Equivalent-circuit diagram of two RSJ-model weak links coupled to a common series resonance circuit.

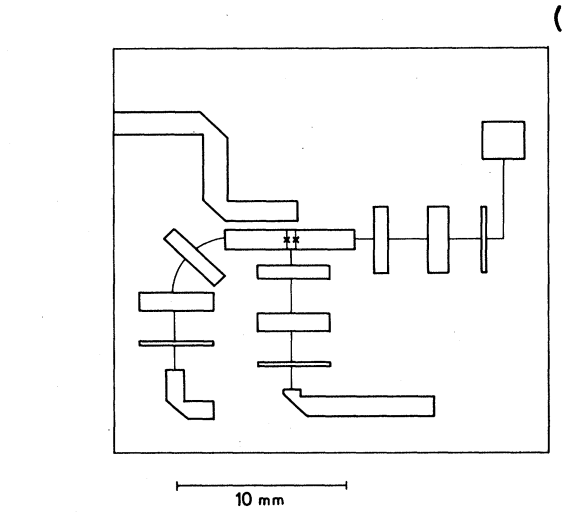

FIG. 28. (a) Example of a thin-film microstrip circuit used to study the coupling of two microbridges to a resonator ($\nu_{\rm res} \approx 10.6$ GHz). The dc bias leads are provided with multisection low-pass filters. The microbridges are shown by crosses. The geometry is due to Finnegan *et al.* (1977). (b) Sample with two indium microbridges in a microstrip resonator mounted in a microwave integrated circuit box (1×1 in.^{2}). The ground plane below the glass substrate is made of copper. Indium press contacts are used to connect the eight thin dc bias leads to the microstrip pads (Bindslev Hansen *et al.*, 1981).

weak links (and neglect noise), the equations describing the behavior of this system are

$$I_1 = I_{c1}\sin\phi_1 + \frac{\hbar}{2eR_1}\frac{d\phi_1}{dt} + i_{\rm res}\ , \tag{4.12}$$

$$I_2 = I_{c2}\sin\phi_2 + \frac{\hbar}{2eR_2}\frac{d\phi_2}{dt} + i_{\rm res}\ , \tag{4.13}$$

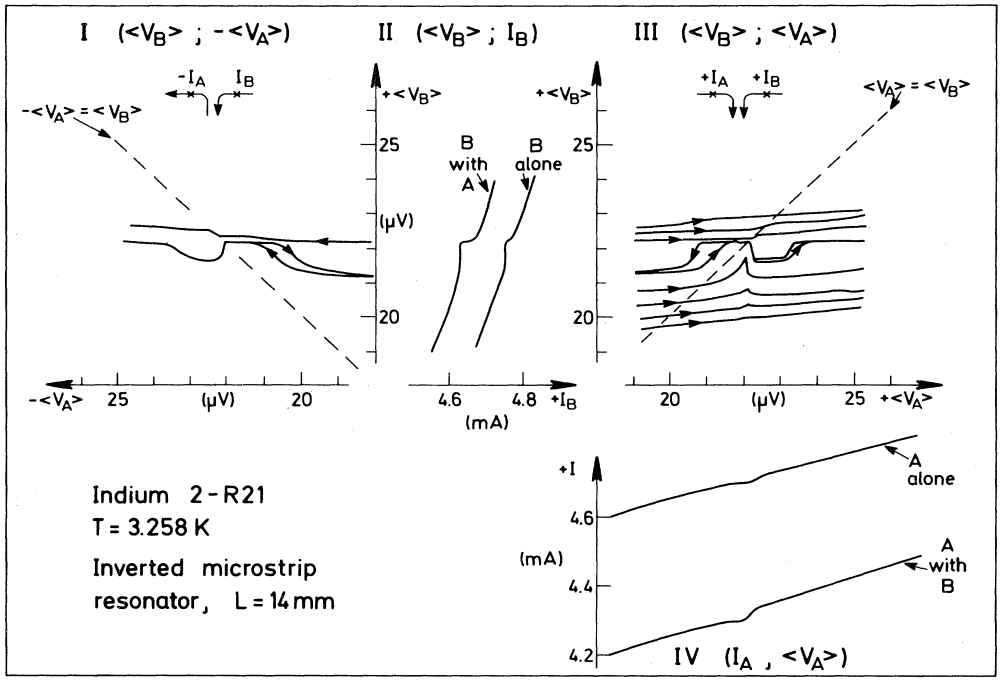

FIG. 29. Experimental curves showing dc voltage-pulling and -locking phenomena for two resonantly coupled indium microbridges (here called A and B). The sample geometry is shown in Fig. 28. The fundamental resonance frequency is 10.6 GHz. The loaded Q is about 300. Parts II and IV show the relevant section of the dc I-V curves for the two bridges separately as well as for both bridges biased around the resonant structure (22 μV). Parts I and III show V_B vs V_A around the same voltage; I_B is fixed and I_A is varied (Bindslev Hansen *et al.*, 1981).

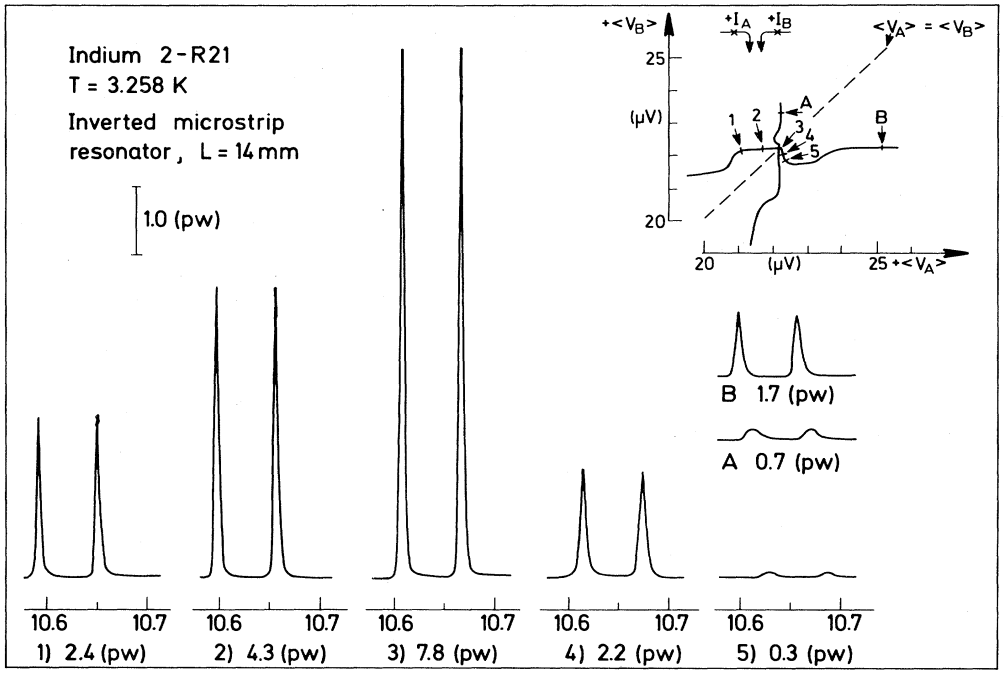

FIG. 30. Experimental radiation traces for the same sample as in Fig. 29. The bias points in the (V_B;V_A) plane for the two bridges are shown in the inset in the upper-right corner. The radiation spectra appear with double peaks due to the superheterodyne detection method used (intermediate frequency: 30 MHz). Spectra A and B give the power radiated at resonance by the two bridges individually. The other five radiation spectra show the coherent radiation around the resonance frequency from both microbridges. In all cases the integrated detected power is given below the spectrum (Bindslev Hansen *et al.*, 1981).

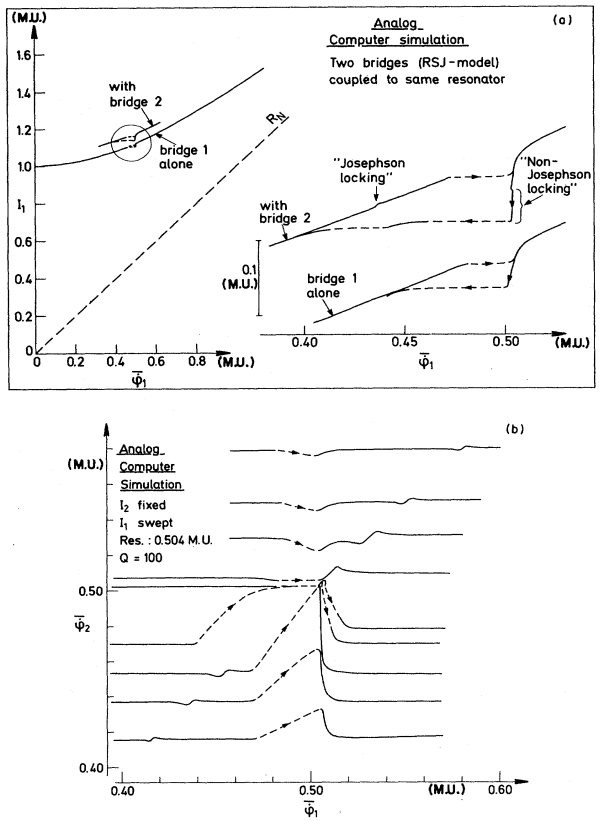

FIG. 31. Analog computer simulation of two RSJ-model weak links coupled to a common-series resonator, Eqs. (4.12)—(4.15). In this simulation $I_{c1}=I_{c2}=1$ and $R_{N1}=R_{N2}=1$, the unloaded Q is 100. For the time scaling used $\nu_{\rm res}=783$ Hz$=0.504$ machine units (M.U.). (a) The I-V characteristic $(I_1,\bar{\phi}_1)$ for one bridge alone and for one bridge with the other biased at resonance (displaced curve). The hysteresis (broken lines) around the self-induced resonance step is a consequence of the current control. (b) The simulated curves of V_1 vs V_2 $(\bar{\phi}_1;\bar{\phi}_2)$ around the resonance frequency (only sweeps with increasing I_1 and I_2 fixed). Both Josephson and non-Josephson locking are seen in the simulation [cf. (a)] (Bindslev Hansen *et al.*, 1981).

$$V_{\rm res}=\frac{\hbar}{2e}\left[\frac{d\phi_1}{dt}+\frac{d\phi_2}{dt}\right]=V_L+V_r+V_c$$

$$=LC\frac{d^2V_c}{dt^2}+RC\frac{dV_c}{dt}+V_c\ , \tag{4.14}$$

$$i_{\rm res}=C\frac{dV_c}{dt}\ . \tag{4.15}$$

This set of four coupled equations is not analytically tractable. Dai and Kao (1980,1981a,1981b) have solved it numerically in a first harmonic approximation and found the voltage-locking curves for a number of different cases with two dissimilar weak links. The full system of equations has also been simulated on an analog computer using an appropriate time scaling ($\times 10^{-11}$) so as also to include the effect of the higher harmonics in the Josephson oscillators (Bindslev Hansen *et al.*, 1981). Dai and Kao (1981) have also treated the case of N almost identical series-connected junctions coupled to a common resonator. They found a typical allowed variation in the critical currents of a few percent (provided the resistance in the pads connecting the bridges is negligible).

Historically, the first unambiguous observation of coherent coupling between Josephson junctions was in fact made on a resonant system. It was a pair of large-area lead tunnel junctions which happened to have internal geometrical resonances that coincided in frequency ($\nu\approx 9$ GHz, $Q\approx 110$) (Finnegan *et al.*, 1972,1977). At the common resonance frequency, coherent radiation was observed from the two junctions. We note that this coupling scheme involving two coupled parallel-resonance circuits differs from the one discussed above.

A system which is a practical realization of the circuit drawn in Fig. 27 is shown in Fig. 28 (Bindslev Hansen *et al.*, 1981). It consists of two indium microbridges coupled to a common resonator consisting of a section of 50-Ω microstrip transmission line.[9]

Some experimental results on such a system are reproduced in Figs. 29 and 30. In Fig. 29 the self-induced step structures in the I-V characteristics of the two bridges (here called A and B) and the dc voltage-pulling and -locking effects are shown.

The phase locking of the Josephson oscillations at the resonance frequency is shown in Fig. 30 for the same sample as in Fig. 29 at a number of points in the $(\bar{V}_A;\bar{V}_B)$ plane around the self-induced step structures and also for the two bridges, radiating alone, individually. The total power radiated when both bridges are biased and locked together on resonance is about 70% more than the expected coherent in-phase total power [expected $P_{A+B}=(\sqrt{P_A}+\sqrt{P_B})^2=4.6$ pW, measured $P_{A+B}=7.8$ pW (spectrum 3)]. Moreover, the linewidth is narrowed down when both bridges are running coherently in phase. These two phenomena are due to a regenerative increase of the effective Q of the resonator when both bridges are exciting the resonance. Both of these effects were also reported by Stern *et al.* (1978,1981) for two microbridges coupled via a waveguide resonator.

Finally, Fig. 31 shows some of the results of analog computer simulations (Hansen *et al.*, 1981). The general features on the dc voltage-pulling and -locking effects seen in the $(\bar{\phi}_1;\bar{\phi}_2)$ plot [Fig. 31(b)] are in fact very similar to the experimental results (Fig. 29, part III). In addition to the strong coupling at the resonance frequency ("non-Josephson" locking), the simulation also shows locking ("Josephson" locking) when $\dot{\bar{\phi}}_1=\dot{\bar{\phi}}_2$ in a wide band around

[9]This is the microstrip used by Finnegan *et al.* (1977,1978) in attempts to couple two tunnel junctions via an external resonator. The complex interaction between the internal and the external resonances made achieving such a coupling impossible. This problem is not encountered with low-capacitance weak links (any internal resonances would here be shifted to much higher frequencies).

the resonance frequency. This interaction also goes via the transmission line, which off resonance acts as a passive filter. Experimentally, this type of locking is indeed observed in resonant systems, as may be seen in Fig. 29, part I, just above the resonance.

V. LARGE ARRAY SYSTEMS

Large arrays of parallel- and/or series-connected Josephson junctions have been studied for two main reasons:

(1) to construct high-frequency devices based on coherent ac Josephson effects in the junctions of the array; and

(2) to investigate the nature of the two-dimensional system of magnetic flux vortices associated with the superconducting screening currents in the multiply connected array system.

In a sense, these two approaches to the behavior of large Josephson arrays are complementary. One is concerned with the dynamic interaction between the high-frequency oscillations in the junctions through coupling currents flowing in the array system. In the other approach the interest is centered on the interaction between the lines of quantized magnetic flux, the flux vortices, that are linked to the screening currents flowing in the array.

Recently most of the work on large arrays has been focused on the discrete two-dimensional vortex lattice and its behavior. This field, which includes the observations of a vortex-unbinding (Kosterlitz-Thouless) transition as well as interesting commensuration effects in an external magnetic field, is growing rapidly and deserves a review of its own. Here we will limit ourselves to mentioning that experimental work on large two-dimensional Josephson array systems has been reported by Sanchez *et al.* (1981), Resnick *et al.* (1981), Voss and Webb (1982), and Abraham *et al.* (1982) [see also Webb *et al.* (1983) and Tinkham *et al.* (1983)], and that related collective flux line behavior in thickness-modulated superconducting thin films has been observed by Martinoli (1978) and by Fiory *et al.* (1978) [see also Gubser *et al.* (1980)]. The connection to inhomogeneous (granular) superconducting films has also been investigated (Davidson *et al.*, 1981).

The high-frequency behavior of *large* arrays of Josephson junctions has been treated theoretically along the same lines as described previously for long-range coupling in *smaller* array systems with two junctions: *broadband interaction* (Nerenberg *et al.*, 1981; Likharev *et al.*, 1981) and *resonant, narrow-band coupling* (Khlus *et al.*, 1979, and Dai and Kao, 1980). Naturally, in the large, multijunction arrays the same interaction mechanisms, which exist between two junctions, come into play, and furthermore collective, long-range phenomena and flux quantization become of paramount importance in these large arrays.

For many device applications single Josephson junctions are of limited use, due to the problems discussed above in Sec. I.C. Coherently working arrays of many junctions have therefore been used or suggested for a number of devices: (1) *voltage standards* (Finnegan *et al.*, 1975; Finnegan and Wahlsten, 1978; Levinsen *et al.*, 1977; Sullivan *et al.*, 1979; Koyanagi *et al.*, 1979; Kautz, 1980; Kobayashi *et al.*, 1983); (2) *parametric amplifiers* (Parrish *et al.*, 1974; Feldman *et al.*, 1975; Chiao *et al.*, 1976; Wahlsten *et al.*, 1978; Rudner *et al.*, 1979; Goodall *et al.*, 1979; Levinsen *et al.*, 1980) and (3) *Josephson mixers* (Claasen *et al.*, 1978). A number of different fabrication techniques have been suggested in these papers. Other articles on fabrication techniques for large arrays have been published by Clark (1968,1973), Tsang *et al.* (1974), Mooij *et al.* (1974), Palmer *et al.* (1974), Lindelof *et al.* (1979), and Lukens *et al.* (1979).

Most of the coupling schemes described above for two Josephson elements have been applied to construct large coherent arrays or to explain the behavior of such systems.

(1) *Coupling via a Fabry-Perot resonator* (Clark, 1968,1970,1971,1973,1974; Repici *et al.*, 1972); *or via a resonant microstrip or slot line structure* (Bindslev Hansen *et al.*, 1981; Davidson, 1981).

(2) *Quasiparticle coupling* (see Fig. 32) (Palmer *et al.*, 1974,1975,1977; Artemenko *et al.*, 1978,1979).

(3) *SQUID-loop coupling* (Clark *et al.*, 1975,1976; Frank *et al.*, 1978; Silver, 1979; Sandell *et al.*, 1979b; Bindslev Hansen *et al.*, 1981).

(4) *RL-loop coupling* (see Fig. 33) (Sandell *et al.*, 1979a,1979b; and Jain *et al.*, 1980; Jain, Mankiewich, and Lukens, 1980).

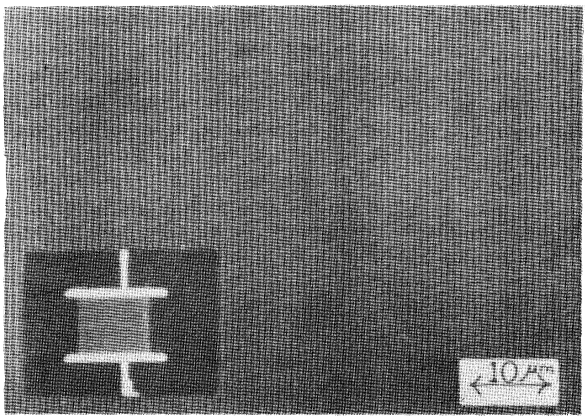

FIG. 32. Reflection microphotograph of a portion of a series-connected array of proximity-effect microbridges (Palmer *et al.*, 1974). The junctions are the dark lines separated by narrow (lighter) superconducting regions. Spacing (center to center) of the bridges is 0.7 μm, the superconducting material is 30 nm niobium/tantalum film. The bias current flows in the horizontal direction. The inset shows a low-magnification view of the whole array: the white area is the sapphire substrate, the dark is the "strong" film (high T_c), and the gray area is 200 bridges in series.

The last of these couplings schemes has so far been the most successful. Jain *et al.* (1980) and Jain, Mankiewich, and Lukens (1980) obtained up to 5-nW output power at 10 GHz over a linewidth of about 1 MHz. This array consisted of 99 microbridges biased in a dc-parallel/ac-series-connected array configuration; see Fig. 33.

It is worth noting that for many applications where the Josephson array is pumped by an external microwave source (voltage standards, parametric amplifiers, mixers) it is possible in this way to synchronize all the oscillating junctions into a coherent state. For such applications it is therefore not necessary to construct arrays in which an internal high-frequency interaction mechanism ensures an intrinsic coherent state. For these devices to work well it is, however, necessary to construct series-connected arrays of almost identical junctions—for instance, Claasen *et al.*

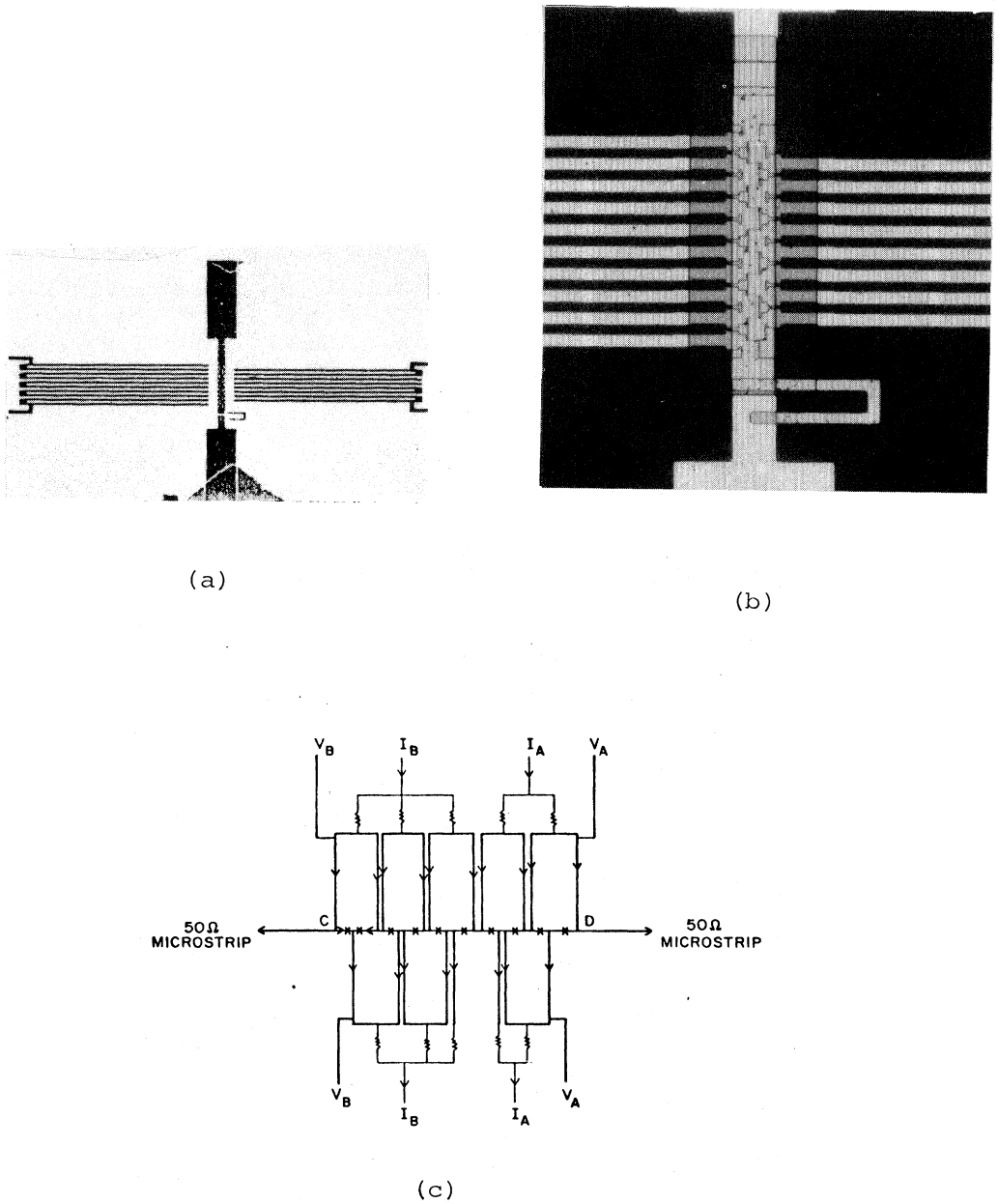

FIG. 33. (a) and (b): Two views of an array of 10 indium microbridges made using electron-beam lithography technique (Jain *et al.*, 1980a,1980b). The distance between the bridges is 10 μm. The bridges are placed in a dc-parallel/ac-series configuration as discussed in the text. In the view on the left, the connections of the array to the 50-Ω microstrips on the top and bottom are visible, as are the SQUID loops and the bias leads on the sides. The bridges lie under the central bar, and are too small to be seen even in the magnified view on the right. The small loop towards the right of the array constitutes the inductance of the *RL*-feedback loop. (c) Schematic of the 10 bridge array. The feedback *RL* loop is not shown. It is connected between the points *C* and *D*. The microbridges are denoted by ×'s. The separation into two sections *A* and *B* is also shown.

(1978) found, theoretically, a maximum allowed spread of 1% for the junction parameters in a mixer array. Therefore, as long as the fabrication of a large number of highly uniform junctions remains a technological problem, dc-parallel/ac-series-connected array configurations will be useful also for these applications.

The dc-parallel/ac-series arrays have been made in order to circumvent the problem of differences in the voltage (frequency) across the nonuniform Josephson junctions in a (dc-) series-connected array; cf. Sec. II.B.1. The use of suitable reactive decoupling circuit elements allows the junctions to be connected in parallel at dc while maintaining an rf-series configuration—i.e., the same microwave current passes through all the junctions (Lindelof *et al.*, 1979; Likharev, 1979; Sandell *et al.*, 1979b; Jain *et al.*, 1980; Jain, Mankiewich, and Lukens, 1980). Such a configuration, however, poses new problems of its own (see Sec. II.B.2). When biased in parallel, loops are formed that together with the junctions constitute SQUID's. Unless measures are taken to minimize the effect of flux quantization within these SQUID loops, the relative phases of the oscillating currents through the junctions will be modulated by the magnetic flux linking the loops. In practice, these flux-induced phase shifts will always destroy the desired overall in-phase coherent oscillation. The solution to this problem lies in quenching the circulating high-frequency SQUID currents. This was done by Jain *et al.* (1980) and Jain, Mankiewich, and Lukens (1980) by making the loop inductances so large that the amplitudes of these currents fell below the level of the ac coupling current.

A geometry resulting from these considerations is shown in Fig. 33. The results by Jain *et al.* (1980) and Jain, Mankiewich, and Lukens (1980) are indeed very encouraging and give promise for the ac Josephson effect working at hitherto unseen power levels, thereby making the effect more useful for device applications.

ACKNOWLEDGMENTS

We are indebted to H. Højgaard Jensen for his support and encouragement and to the "Josephson group" at the Technical University, Lyngby, for their continuing cooperation. The generous financial support from the Danish Natural Science Research Council and from the Carlsberg Foundation is gratefully acknowledged.

REFERENCES

Abraham, D. W., C. J. Lobb, M. Tinkham, and T. M. Klapwijk, 1982, Phys. Rev. B **26**, 5268.

Amatuni, L. E., V. N. Gubankov, A. V. Zaitsev, and G. A. Ovsyannikov, 1982, Zh. Eksp. Teor. Fiz. **83**, 1851 [Sov. Phys.—JETP **56**, 1070 (1982)].

Ambegaokar, V., and M. R. Arai, 1981, Appl. Phys. Lett. **39**, 763.

Ambegaokar, V., and A. Baratoff, 1963, Phys. Rev. Lett. **10**, 486; **11**, 104(E) (1963).

Aponte, J. M., and M. Tinkham, 1983, J. Low Temp. Phys. **51**, 189.

Artemenko, S. N., and A. F. Volkov, 1979, Usp. Fiz. Nauk **128**, 3 [Sov. Phys.—Usp. **22**, 295 (1979)].

Artemenko, S. N., A. F. Volkov, and A. V. Zaitsev, 1978, J. Phys. (Paris) Colloq. **39**, C6-588.

Aslamazov, L. G., and A. I. Larkin, 1969, Zh. Eksp. Teor. Fiz. Pis'ma Red. **9**, 150 [JETP Lett. **9**, 87 (1969)].

Bindslev Hansen, J., 1981, "Static and dynamic interactions in arrays of superconducting Josephson weak links," Ph.D. thesis (University of Copenhagen).

Bindslev Hansen, J., 1982, Phys. Scr. **25**, 844.

Bindslev Hansen, J., T. F. Finnegan, and P. E. Lindelof, 1981, IEEE Trans. Magn. **MAG-17**, 95.

Bindslev Hansen, J., and P. E. Lindelof, 1980, "Nonequilibrium phenomena in Josephson junctions," in *Proceedings of the 2nd SQUID Conference,* edited by H. D. Hahlbohm and H. Lübbig (Walter de Gruyter, Berlin), p. 29.

Blackburn, J. A., 1983, J. Low Temp. Phys. **50**, 475.

Blackburn, J. A., B. B. Schwartz, and A. Baratoff, 1972, Phys. Lett. **42A**, 31.

Blackburn, J. A., B. B. Schwartz, and A. Baratoff, 1975, J. Low Temp. Phys. **20**, 523.

de Bruyn Ouboter, R., and A. Th. A. M. De Waele, 1970, "Superconducting point contacts weakly connecting two superconductors," in *Progress in Low Temperature Physics,* edited by C. J. Gorter (North-Holland, Amsterdam), Vol. 6, p. 243.

Carlson, R. V., and A. M. Goldman, 1975, Phys. Rev. Lett. **34**, 11.

Carlson, R. V., and A. M. Goldman, 1976, J. Low Temp. Phys. **25**, 67.

Chi, C. C., L. Krusin-Elbaum, and C. C. Tsuei, 1981, Physica **108B**, 1085.

Chiao, R. Y., and P. T. Parrish, 1976, J. Appl. Phys. **47**, 2639.

Claasen, J. H., and P. L. Richards, 1978, J. Appl. Phys. **49**, 4117.

Clark, T. D., 1968, Phys. Lett. **27A**, 585.

Clark, T. D., 1971a, "Interaction of microwaves with point contact Josephson junction arrays," in *Proceedings of the 12th Conference on Low-Temperature Physics, Kyoto, 1970,* edited by E. Kanda (Academic Press of Japan, Tokyo), p. 449.

Clark, T. D., 1971b, Physica **55**, 432.

Clark, T. D., 1973, Phys. Rev. B **8**, 137.

Clark, T. D., 1974, Rev. Phys. Appl. **9**, 207.

Clark, T. D., and P. E. Lindelof, 1975, "Analogous computer simulation of the phase-locked, collectively driven state in two-dimensional Josephson junction arrays," in *Low Temperature Physics—LT14,* edited by M. Krusius and M. Vuorio (North-Holland, Amsterdam), Vol. 4 (Techniques and Special Topics), p. 218.

Clark, T. D., and P. E. Lindelof, 1976, Appl. Phys. Lett. **29**, 751.

Daalmans, G. M., T. M. Klapwijk, and J. E. Mooij, 1977, IEEE Trans. Magn. **MAG-13**, 719.

Dai, Y.-D., and Y. H. Kao, 1980, "Coherent radiation of Josephson junction arrays," in *Proceedings of the 2nd SQUID Conference,* edited by H. D. Hahlbohm and H. Lübbig (Walter de Gruyter, Berlin), p. 921.

Dai, Y.-D., and Y. H. Kao, 1981a, J. Appl. Phys. **52**, 4135.

Dai, Y.-D., and Y. H. Kao, 1981b, J. Low Temp. Phys. **43**, 411.

Dai, Y.-D., W. J. Yeh, and Y. H. Kao, 1982, J. Low Temp. Phys. **48**, 373.

Davidson, A., 1981, IEEE Trans. Magn. **MAG-17**, 103.

Davidson, A., and C. C. Tsuei, 1981, Physica **108B**, 1243.

Deakin, A. S., and M. A. H. Nerenberg, 1982, Phys. Rev. B **25**, 1559.
Deakin, A. S., and M. A. H. Nerenberg, 1983, Phys. Rev. B **27**, 6954.
Deminova, G. F., and A. S. Kovalenko, 1979, IEEE Trans. Magn. **MAG-15**, 291.
De Waele, A. Th. A. M., W. H. Kraan, and R. de Bruyn Ouboter, 1968, Physica **40**, 302.
Dolan, G. J., and L. D. Jackel, 1977, Phys. Rev. Lett. **39**, 1628.
Faris, S. M., S. I. Raider, W. J. Gallagher, and R. E. Drake, 1983, IEEE Trans. Magn. **MAG-19**, 1293.
Feldman, M. H., P. T. Parrish, and R. Y. Chiao, 1975, J. Appl. Phys. **46**, 4031.
Feynman, R., 1965, *The Feynman Lectures on Physics* (Addison-Wesley, Reading), Vol. 3.
Finnegan, T. F., L. B. Holdeman, and S. Wahlsten, 1977, IEEE Trans. Magn. **MAG-13**, 392.
Finnegan, T. F., and S. Wahlsten, 1972a, Appl. Phys. Lett. **21**, 541.
Finnegan, T. F., and S. Wahlsten, 1972b, "Microwave emission from coupled Josephson junctions," in *Low Temperature Physics—LT13 (1972),* edited by K. D. Timmerhaus, W. J. O'Sullivan, and E. F. Hammel (Plenum, New York), Vol. 3, p. 272.
Finnegan, T. F., and S. Wahlsten, 1978, Physica **94B**, 219.
Finnegan, T. F., J. Wilson, and J. Toots, 1975, IEEE Trans. Magn. **MAG-11**, 821.
Fiory, A. T., A. F. Hebard, and S. Somekh, 1978, Appl. Phys. Lett. **32**, 73.
Frank, D., H. A. Notarys, and J. E. Mercercau, 1978, "Fluxoid coupling between superconducting weak links," preprint, California Institute of Technology.
Garvey, S., S. Logan, R. Rowe, and W. A. Little, 1983, Appl. Phys. Lett. **42**, 1048.
Giaever, I., 1965, Phys. Rev. Lett. **14**, 904.
Giovannini, B., L. Weiss-Parmeggiani, and B. T. Ulrich, 1978, Helv. Phys. Acta **51**, 69.
Goodall, F., 1979, IEEE Trans. Magn. **MAG-15**, 458.
Gray, K. E., 1978, Appl. Phys. Lett. **32**, 392.
Gray, K. E., 1981, Ed., *Non-Equilibrium Superconductivity, Phonons, and Kapitza Boundaries* (Plenum, New York).
Greiner, J. H., C. J. Kircher, S. P. Klepner, S. K. Lahiri, A. J. Warnecke, S. Basavaiah, E. T. Yen, J. M. Baker, P. R. Brosius, H.-C. W. Huang, M. Murakami, and I. Ames, 1980, IBM J. Res. Dev. **24**, 195.
Gubankov, V. N., L. S. Kuz'min, K. K. Likharev, and V. K. Semenov, 1975, Zh. Eksp. Teor. Fiz. **68**, 2301 [Sov. Phys.—JETP **41**, 1150 (1976)].
Gubser, D. V., T. L. Francavilla, S. Wolf, and J. Laibowitz, 1980, Eds., *Inhomogeneous Superconductors—1979,* AIP Conference Proceedings No. 58 (AIP, New York).
Gupta, K. C., R. Garg, and I. J. Bahl, 1979, *Microstrip Lines and Slotlines* (Artech House, Dedham).
Harris, R. E., and C. A. Hamilton, 1978, "Fast superconducting instruments," in *Future Trends in Superconductive Electronics,* AIP Conference Proceedings No. 44, edited by B. S. Deaver, Jr., C. M. Falco, J. H. Harris, and S. A. Wolf (AIP, New York), p. 448.
Hebard, A. F., and R. H. Eich, 1978, J. Appl. Phys. **49**, 338.
Hohenwarter, G. K., and J. B. Beyer, 1981, IEEE Trans. Magn. **MAG-17**, 826.
Howard, W., and Y. H. Kao, 1975, "Current-phase relationship of coupled semiconducting weak links," in *Low Temperature Physics—LT14,* edited by M. Krusius and M. Vuorio (North-Holland, Amsterdam), Vol. 4 (Techniques and Special Topics), p. 144.
Hunt, B. D., and R. A. Buhrman, 1983, IEEE Trans. Magn. **MAG-19**, 1155.
Imry, Y., and L. S. Schulman, 1978, J. Appl. Phys. **49**, 749.
Jain, A. K., A. M. Kadin, J. E. Lukens, P. Mankiewich, R. H. Ono, and D. B. Schwartz, 1980, "Microwave generation using coherent arrays of Josephson junctions," in *Proceedings of the 2nd SQUID Conference,* edited by H. D. Hahlbohm and H. Lübbig (Walter de Gruyter, Berlin), p. 939.
Jain, A. K., A. M. Kadin, J. E. Lukens, P. Mankiewich, R. H. Ono, and D. B. Schwartz, 1981, IEEE Trans. Magn. **MAG-17**, 99.
Jain, A. K., K. K. Likharev, J. E. Lukens, and J. E. Sauvegeau, 1982, Appl. Phys. Lett. **41**, 556; **42**, 305(E) (1983).
Jain, A. K., K. K. Likharev, J. E. Lukens, and J. E. Sauvegeau, 1982, preprint, State University of New York at Stony Brook.
Jain, A. K., J. E. Lukens, Kin Li, R. D. Sandell, and C. Varmazis, 1979, "Current-voltage characteristic of interacting Josephson junctions," in *Inhomogeneous Superconductors,* AIP Conference Proceedings No. 58, edited by D. Gubser *et al.* (AIP, New York), p. 265.
Jain, A. K., P. Mankiewich, and J. E. Lukens, 1980, Appl. Phys. Lett. **36**, 774.
Jillie, D. W., 1976, "Interactions between coupled thin-film microbridge Josephson junctions," Ph.D. thesis (State University of New York at Stony Brook).
Jillie, D. W., 1981, Physica **107B**, 741.
Jillie, D. W., J. E. Lukens, and Y. H. Kao, 1975, IEEE Trans. Magn. **MAG-11**, 671.
Jillie, D. W., J. E. Lukens, and Y. H. Kao, 1977a, Phys. Rev. Lett. **38**, 915.
Jillie, D. W., J. E. Lukens, and Y. H. Kao, 1977b, IEEE Trans. Magn. **MAG-13**, 578.
Jillie, D. W., J. E. Lukens, Y. H. Kao, and G. J. Dolan, 1976, Phys. Lett. **55A**, 381.
Jillie, D. W., M. A. H. Nerenberg, and J. A. Blackburn, 1980, Phys. Rev. B **21**, 125.
Josephson, B. D., 1962, Phys. Lett. **1**, 251.
Josephson, B. D., 1964, Rev. Mod. Phys. **36**, 216.
Josephson, B. D., 1965, Adv. Phys. **14**, 419.
Kadin, A. M., 1979, "Non-equilibrium phenomena in superconducting phase-slip centers," Ph.D. thesis (Harvard University).
Kadin, A. M., L. N. Smith, and W. J. Skocpol, 1980, J. Low Temp. Phys. **38**, 497.
Kadin, A. M., C. Vermazis, and J. E. Lukens, 1981, Physica **108B**, 159.
Kaplan, S. B., J. R. Kirtley, and D. N. Langenberg, 1977, Phys. Rev. Lett. **39**, 291.
Kautz, R. L., 1980, Appl. Phys. Lett. **36**, 386.
Khlus, V. A., A. S. Rozhavskii, and I. O. Kulik, 1979, Sov. J. Low Temp. Phys. **5**, 169.
Kobayashi, T., K. Hamasaki, N. Kondoh, T. Komata, and T. Yamashita, 1983, Appl. Phys. Lett. **42**, 475.
Koyanagi, M., T. Endo, and A. Nakamura, 1979, "Higher standard voltage generated by multiple Josephson junctions," in *Future Trends in Superconductive Electronics,* AIP Conference Proceedings No. 44, edited by B. C. Deaver, Jr., C. M. Falco, J. H. Harris, and S. A. Wolf (AIP, New York), p. 187.
Krech, W., and H. H. Gross, 1979, Fiz. Nizk. Temp. **5**, 433 [Sov. J. Low Temp. Phys. **5**, 207 (1979)].
Kuzmin, L. S., K. L. Likharev, G. A. Ovsyannikov, 1981, Radio Eng. Electron. Phys. **26**, 102.
Levinsen, M. T., R. Y. Chiao, M. J. Feldman, and B. A. Tuck-

er, 1977, Appl. Phys. Lett. **31**, 776.
Levinsen, M. T., N. F. Pedersen, O. H. Sørensen, B. Dueholm, and J. Mygind, 1980, IEEE Trans. Electron Devices (special issue on Josephson junction devices) **ED-27**, No. 10, p. 1928.
Likharev, K. K., 1979, Rev. Mod. Phys. **51**, 101.
Likharev, K. K., L. S. Kuzmin, and G. A. Ovsyannikov, 1981, IEEE Trans. Magn. **MAG-17**, 111.
Likharev, K. K., and V. K. Semenov, 1972, JETP Lett. **15**, 442.
Lindelof, P. E., 1978, J. Phys. (Paris) Colloq. **39**, C6-1411.
Lindelof, P. E., 1981, Rep. Prog. Phys. **44**, 949.
Lindelof, P. E., and J. Bindslev Hansen, 1977, J. Low Temp. Phys. **29**, 369.
Lindelof, P. E., and J. Bindslev Hansen, 1981, "Short-range interaction between two superconducting weak links," in *Non-Equilibrium Superconductivity, Phonons, and Kapitza Boundaries,* edited by K. E. Gray (Plenum, New York), Chap. 19. p. 593.
Lindelof, P. E., J. Bindslev Hansen, and P. Jespersen, 1979, "Superconducting microbridges and arrays," in *Future Trends in Superconductive Electronics,* AIP Conference Proceedings No. 44, edited by B. S. Deaver, Jr., C. M. Falco, J. H. Harris, and S. A. Wolf (AIP, New York), p. 322.
Lindelof, P. E., J. Bindslev Hansen, J. Mygind, N. F. Pedersen, and O. H. Sørensen, 1977, Phys. Lett. **60A**, 451.
Little, W. A., 1978, in *Applications of Closed-Cycle Cryocoolers to Small Superconducting Devices,* Natl. Bur. Stand. Spec. Publ. **508**, 75.
Lukens, J. E., R. D. Sandell, and C. Varmazis, 1979, "Fabrication of microbridge Josephson junctions using electron beam lithography," in *Future Trends in Superconductive Electronics,* AIP Conference Proceedings No. 44, edited by B. S. Deaver, Jr., C. M. Falco, J. H. Harris, and S. A. Wolf (AIP, New York), p. 298.
Martinoli, P., 1978, Phys. Rev. B **17**, 1175.
Meyer, J. D., and G. von Minnigerode, 1972, Phys. Lett. **38A**, 529.
Meyer, J. D., and R. Tidecks, 1977, Solid State Commun. **24**, 643.
Mineev, M. G., G. S. Mkrtchyan, and V. V. Schmidt, 1981, J. Low Temp. Phys. **45**, 497.
Mooij, J. E., C. A. Gorter, and J. E. Noordam, 1974, Rev. Phys. Appl. **9**, 173.
Nerenberg, M. A. H., J. A. Blackburn, and D. W. Jillie, 1980, Phys. Rev. B **21**, 118.
Neumann, L. G., Y.-D. Dai, and Y. H. Kao, 1981, Appl. Phys. Lett. **39**, 648.
Neumann, L. G., Y.-D. Dai, and Y. H. Kao, 1982, J. Low Temp. Phys. **49**, 457.
Notarys, H. A., and J. E. Mercereau, 1971, Physica **55**, 424.
Octavio, M., and W. J. Skocpol, 1979, J. Appl. Phys. **50**, 3505.
Palmer, D. W., and J. E. Mercereau, 1974, Appl. Phys. Lett. **25**, 467.
Palmer, D. W., and J. E. Mercereau, 1975, IEEE Trans. Magn. **MAG-11**, 667.
Palmer, D. W., and J. E. Mercereau, 1977, Phys. Lett. **61A**, 135.
Parmenter, R. M., 1967, Phys. Rev. **154**, 353.
Parrish, P. T., and R. Y. Chaio, 1974, Appl. Phys. Lett. **25**, 627.
Pethick, C. J., and H. Smith, 1979, Ann. Phys. (N.Y.) **119**, 133.
Pippard, A. B., J. G. Shepherd, and D. A. Tindall, 1970, Proc. R. Soc. London, Ser. A **324**, 17.
Repici, D. J., W. D. Gregory, M. Behravesh, and T. Thompson, 1972, "Radiation generation and detection characteristics of arrays of point-contact Josephson junctions," in *Proceedings of Applications of Superconductors Conference,* Annapolis, IEEE Conf. Rec. NCH0682-5-TABSC, p. 701.
Resnick, J., J. C. Garland, J. T. Boyd, S. Shoemaker, and R. S. Newrock, 1981, Phys. Rev. Lett. **47**, 1542.
Rudner, S., and T. Claeson, 1979, Appl. Phys. Lett. **34**, 711.
Sanchez, D. H., J.-L. Berchier, 1978, J. Low Temp. Phys. **43**, 65.
Sandell, R. D., C. Varmazis, A. K. Jain, and J. E. Lukens, 1979a, "Study of the properties of coherent microbridges coupled by external shunts," in *Future Trends in Superconductive Electronics,* AIP Conference Proceedings No. 44, edited by B. S. Deaver, Jr., C. M. Falco, J. H. Harris, and S. A. Wolf (AIP, New York), p. 327.
Sandell, R. D., C. Varmazis, A. K. Jain, and J. E. Lukens, 1979b, IEEE Trans. Magn. **MAG-15**, 462.
Schmid, A., 1981, "Kinetic equations for dirty superconductors," in *Non-Equilibrium Superconductivity, Phonons, and Kapitza Boundaries,* edited by K. E. Gray (Plenum, New York), Chap. 14, p. 423.
Schmid, A., and G. Schön, 1975a, Phys. Rev. Lett. **34**, 941.
Schmid, A., and G. Schön, 1975b, J. Low Temp. Phys. **20**, 207.
Silver, A. H., 1974, IEEE Trans. Magn. **MAG-15**, 268.
Silver, A. H., D. C. Pridmore-Brown, and J. P. Hurrell, 1981, IEEE Trans. Magn. **MAG-17**, 412.
Silver, A. H., and J. E. Zimmerman, 1967, Phys. Rev. **158**, 423.
Skocpol, W. J., 1981, "Nonequilibrium effects in 1-dim. superconductors," in *Non-Equilibrium Superconductivity, Phonons, and Kapitza Boundaries,* edited by K. E. Gray (Plenum, New York), Chap. 18, p. 559.
Skocpol, W. J., M. R. Beasley, and M. Tinkham, 1974, J. Low Temp. Phys. **16**, 145.
Skocpol, W. J., and L. D. Jackel, 1981, Physica **108B**, 1021.
Sørensen, O. H., N. F. Pedersen, J. Mygind, B. Dueholm, T. F. Finnegan, J. Bindslev Hansen, and P. E. Lindelof, 1981, IEEE Trans. Magn. **MAG-17**, 107.
Stern, M., W. Howard, and Y. H. Kao, 1978, J. Phys. (Paris) Colloq. **39**, C6-577.
Stern, M. B., and Y. H. Kao, 1981, Physica **108B**, 995.
Stuivinga, M., J. E. Mooij, and T. M. Klapwijk, 1981, Physica **108B**, 1023.
Stuivinga, M., C. L. G. Ham, T. M. Klapwijk, and J. E. Mooij, 1983, J. Low Temp. Phys. **53**, 633.
Sullivan, D. B., L. B. Holdeman, and R. J. Soulen, 1978, "The future of superconducting instruments in metrology," in *Future Trends in Superconductive Electronics,* AIP Conference Proceedings No. 44, edited by B. S. Deaver, Jr., C. M. Falco, J. H. Harris, and S. A. Wolf (AIP, New York), p. 171.
Sullivan, D. B., J. E. Zimmerman, and J. T. Ives, 1981, "Operation of a practical SQUID gradiometer in a low-power stirling cryocooler," in *Refrigeration for Cryogenic Sensors and Electronic Systems,* NBS Special Publication No. 607, p. 186.
Tilley, D. R., 1970, Phys. Lett. **33A**, 205.
Tinkham, M., 1979, "Non-Equilibrium superconductivity," in *Festkörperprobleme* (Advances in Solid State Physics), edited by J. Treusch (Vieweg, Braunschweig), Vol. 19, p. 363.
Tinkham, M., and J. Clarke, 1972, Phys. Rev. Lett. **28**, 1366.
Tinkham, M., M. Octavio, and W. J. Skocpol, 1977, J. Appl. Phys. **48**, 1311.
Tinkham, M., D. W. Abraham, and C. J. Lobb, 1983, Phys. Rev. B **28**, 6578.
Tsang, W. T., and S. Wang, 1974, Appl. Phys. Lett. **24**, 519.
Varmazis, C., R. D. Sandell, A. K. Jain, and J. E. Lukens, 1978, Appl. Phys. Lett. **33**, 357.
Voss, R. F., and R. A. Webb, 1982, Phys. Rev. B **25**, 3446.

Vystavkin, A. N., V. N. Gubankov, L. S. Kuz'min, K. K. Likharev, V. V. Migulin, and V. K. Semenov, 1974, Rev. Phys. Appl. **9**, 79.
Wahlsten, S., S. Rudner, and T. Claeson, 1978, J. Appl. Phys. **49**, 4248.
Waldram, J. R., 1975, Proc. R. Soc. London, Ser. A **345**, 231.
Waldram, J. R., 1976, Rep. Prog. Phys. **39**, 751.
Way, Y. C., K. C. Hsu, and Y. H. Kao, 1977, Phys. Rev. Lett. **39**, 1684.
Webb, R. A., R. F. Voss, G. Grinstein, and P. M. Horn, 1983, Phys. Rev. Lett. **51**, 690.
Weiss-Parmeggiani, L., 1982, "Dérivation microscopique de la Fonctionelle de Ginzburg-Landau pour un réseau de jonctions Josephson," Ph.D. thesis (University of Geneva).
Zhang, L., Y.-D. Dai, and Y. H. Kao, 1983, J. Appl. Phys. **54**, 4494.
Zimmerman, J. E., 1980, "Cryogenics for SQUID's," in *Proceedings of the 2nd SQUID Conference,* edited by H. D. Hahlbohm and H. Lübbig (Walter de Gruyter, Berlin), p. 423.

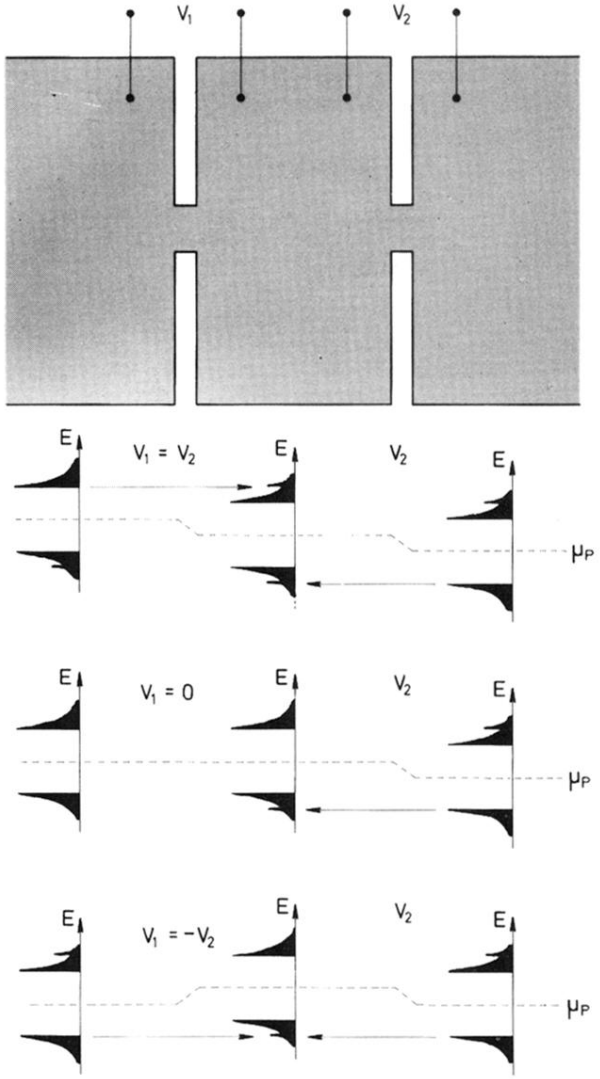

FIG. 16. Qualitative illustration of the asymmetrical quasiparticle dc voltage-locking mechanism. The superconducting film with the two closely spaced microbridges are shown at the top. Below that and with the same x axis, the variation of the pair potential μ_p through the system is shown for three different bias situations (V_2 is constant): $V_1 = V_2$ (series), $V_1 = 0$, and $V_1 = -V_2$ (opposed biased). The quasiparticle distribution in the three regions with the injected peaks due to the diffusive currents is also shown. The dc voltage locking occurs only for the opposed-biased current configuration (lowest picture), as discussed in the text (Lindelof *et al.*, 1981).

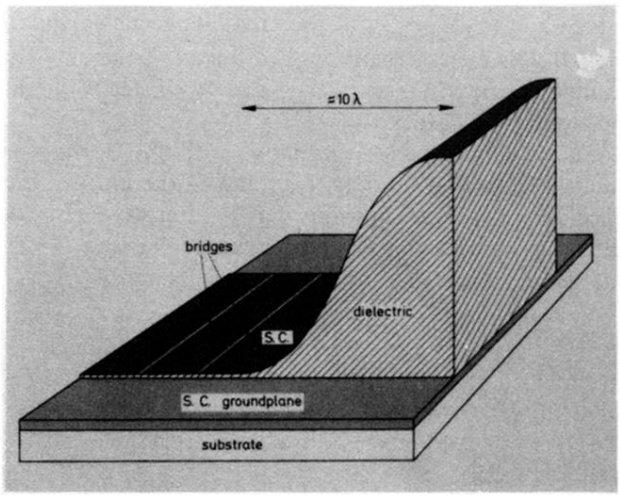

FIG. 26. Drawing showing *in principle* how to couple two Josephson weak links via a low-impedance microstrip transmission line with a large W/H ratio (see Fig. 25) and how to use a tapered impedance-transformer section of the microstrip to establish a good coupling to an external high-impedance transmission line. Since the width of the line should not exceed $\lambda/2$, the 10λ tapered section is considerably compressed in the drawing.

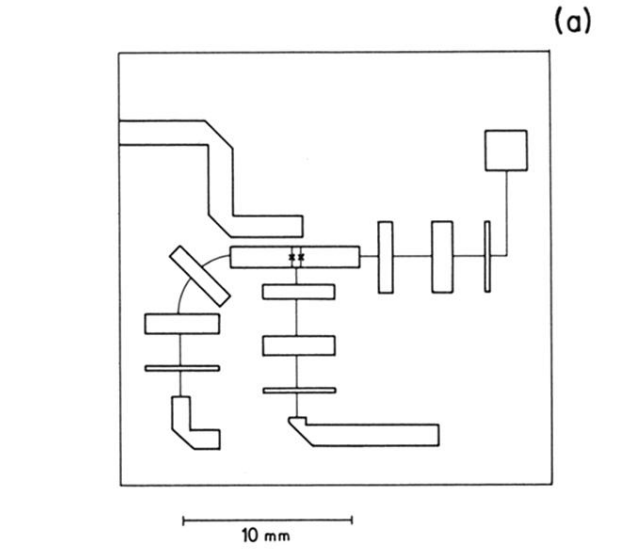

FIG. 28. (a) Example of a thin-film microstrip circuit used to study the coupling of two microbridges to a resonator ($\nu_{res} \approx 10.6$ GHz). The dc bias leads are provided with multisection low-pass filters. The microbridges are shown by crosses. The geometry is due to Finnegan *et al.* (1977). (b) Sample with two indium microbridges in a microstrip resonator mounted in a microwave integrated circuit box (1×1 in.^{2}). The ground plane below the glass substrate is made of copper. Indium press contacts are used to connect the eight thin dc bias leads to the microstrip pads (Bindslev Hansen *et al.*, 1981).

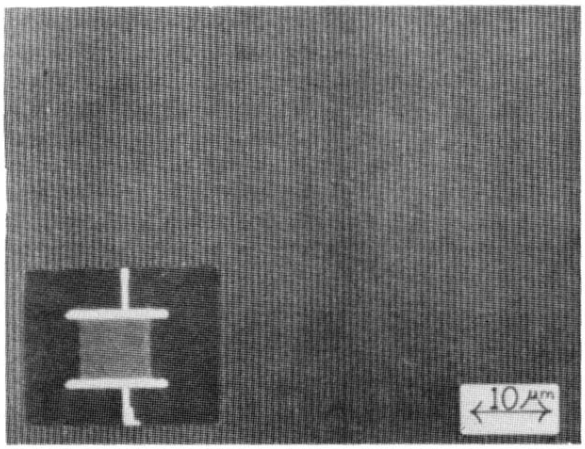

FIG. 32. Reflection microphotograph of a portion of a series-connected array of proximity-effect microbridges (Palmer *et al.*, 1974). The junctions are the dark lines separated by narrow (lighter) superconducting regions. Spacing (center to center) of the bridges is 0.7 μm, the superconducting material is 30 nm niobium/tantalum film. The bias current flows in the horizontal direction. The inset shows a low-magnification view of the whole array: the white area is the sapphire substrate, the dark is the "strong" film (high T_c), and the gray area is 200 bridges in series.

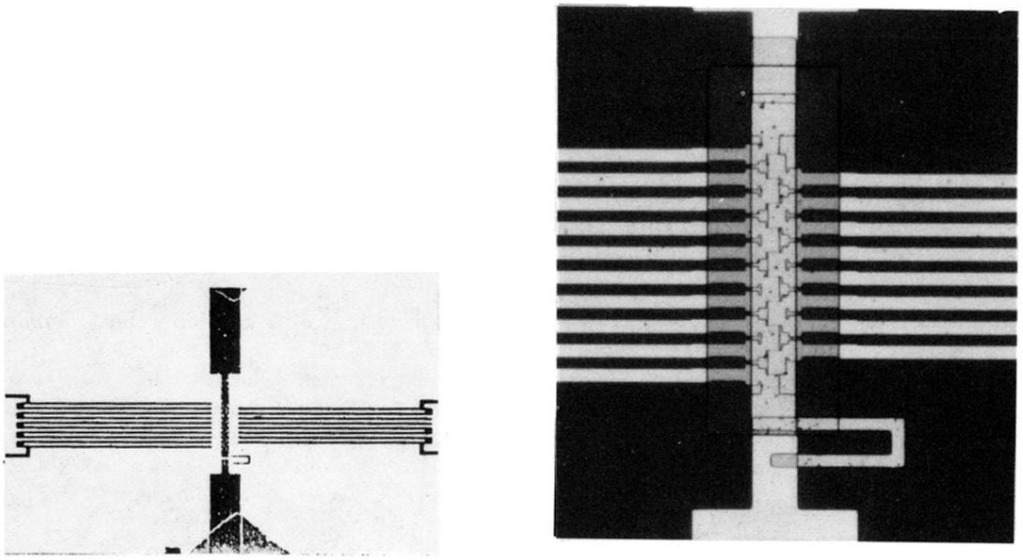

(a)

(b)

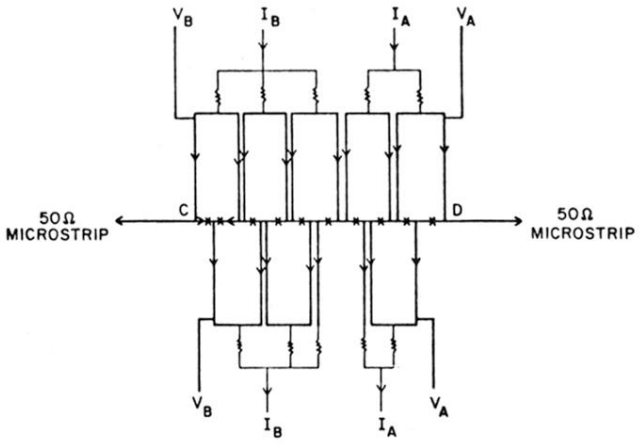

(c)

FIG. 33. (a) and (b): Two views of an array of 10 indium microbridges made using electron-beam lithography technique (Jain *et al.*, 1980a,1980b). The distance between the bridges is 10 μm. The bridges are placed in a dc-parallel/ac-series configuration as discussed in the text. In the view on the left, the connections of the array to the 50-Ω microstrips on the top and bottom are visible, as are the SQUID loops and the bias leads on the sides. The bridges lie under the central bar, and are too small to be seen even in the magnified view on the right. The small loop towards the right of the array constitutes the inductance of the *RL*-feedback loop. (c) Schematic of the 10 bridge array. The feedback *RL* loop is not shown. It is connected between the points *C* and *D*. The microbridges are denoted by $\times$'s. The separation into two sections *A* and *B* is also shown.

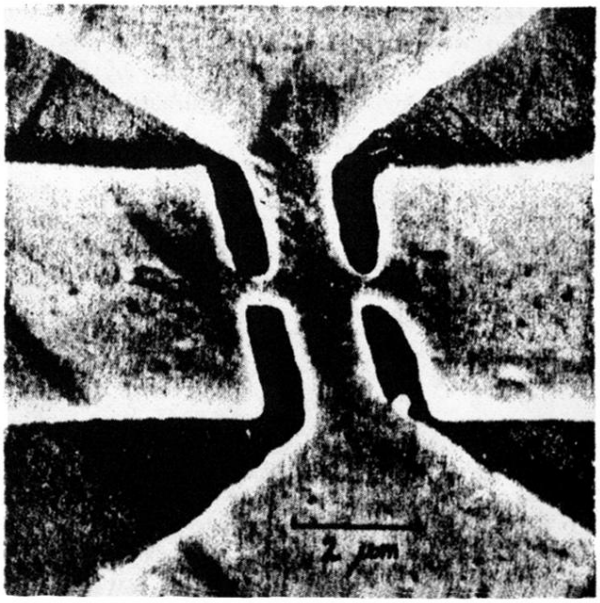

FIG. 4. Scanning electron microscope picture of two indium thin-film microbridges made with electron beam lithography technique (Jillie *et al.*, 1975). The light areas are 100 nm indium film. The bridge separation d is here 1.2 μm.

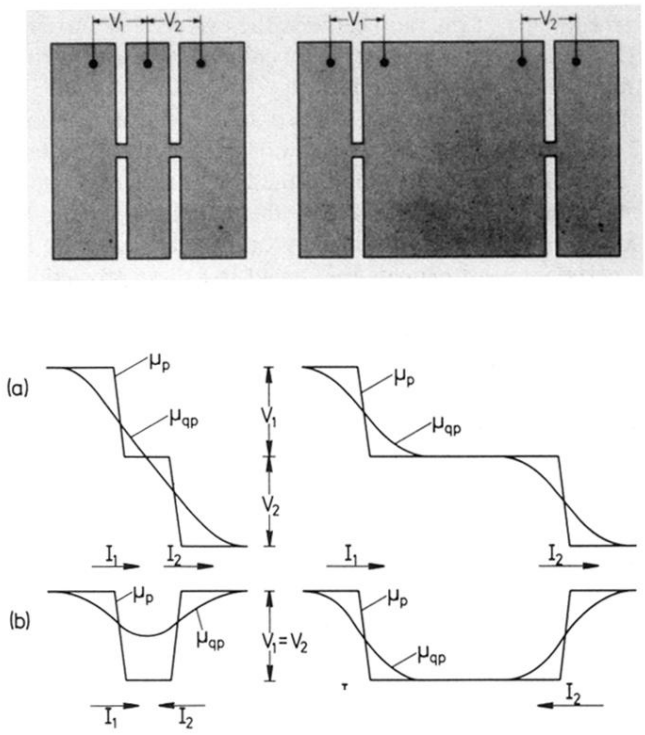

FIG. 9. Qualitative picture of the instantaneous variation of the pair potential μ_p and the quasiparticle potential μ_{qp} in the region around two closely spaced microbridges (shown in the upper part of the figure). The variations are shown for two different interbridge spacings and for both current configurations, (a) series biased, and (b) opposed biased (Lindelof *et al.*, 1981).